arXiv:2101.03530v1 [physics.chem-ph] 10 Jan 2021

Transformative Applications of Machine Learning for Chemical Reactions

Markus Meuwly*,†,‡

†*Department of Chemistry, University of Basel, Klingelbergstrasse 80, 4056 Basel, Switzerland*

‡*Department of Chemistry, Brown University, Providence/RI, USA*

E-mail: m.meuwly@unibas.ch

Abstract

Machine learning techniques applied to chemical reactions has a long history. The present contribution discusses applications ranging from small molecule reaction dynamics to platforms for reaction planning. ML-based techniques can be of particular interest for problems which involve both, computation and experiments. For one, Bayesian inference is a powerful approach to include knowledge from experiment in improving computational models. ML-based methods can also be used to handle problems that are formally intractable using conventional approaches, such as exhaustive characterization of state-to-state information in reactive collisions. Finally, the explicit simulation of reactive networks as they occur in combustion has become possible using machine-learned neural network potentials. This review provides an overview of the questions that can and have been addressed using machine learning techniques and an outlook discusses challenges in this diverse and stimulating field. It is concluded that ML applied to chemistry problems as practiced and conceived today has the potential to transform the way with which the field approaches problems involving chemical reactions, both, in research and academic teaching.

1 Introduction

The prediction of chemical reaction outcomes in terms of products, yields, or reaction rates from computations is a formidable undertaking. Characterizing and understanding chemical transformations is at the heart of chemistry and provides the necessary information about mechanisms and efficiencies of such processes. A quantitative understanding of the speed and efficiency of chemical reactions pertains to, but is not limited to, fields as diverse as atmospheric,[1] combustion,[2] or astrophysical reactions[3] to explosions and enzymatic[4] or organic reactions.[5] It is both of interest to unravel mechanistic underpinnings of known and well-characterized reactions and to predict reaction outcomes based on physically based or physics-inspired models[6] or on high-accuracy PESs.[7–9]

If one is interested in following bond breaking and bond formation in time and space, there are in general two possibilities based on dynamics simulations: those directly and explicitly using quantum mechanical (QM) calculations for the total (electronic) energy and methods based on representations of these energies such as (parametrized) empirical force fields or - as done more recently - based on machine learning. Empirical energy functions represent the potential energy surface (PES) as a computable function for given atomic coordinates whereas QM-based methods solve the electronic Schrödinger equation directly for every configuration $\vec{x}$ of the system for which it is required. QM-based methods[10] provide the most general framework for investigating the dynamics of chemical reactivity without preconceived molecular structures or reaction mechanisms. However, there are certain limitations which are due to the computational approach *per se* (such as the speed and efficiency of the method) or due to practical aspects of quantum chemistry (e.g. basis set superposition error, the convergence of the Hartree-Fock wavefunction to the desired electronic state for arbitrary geometries, or the choice of a suitable active space irrespective of molecular geometry). Improvements and future avenues for making QM-based approaches even more broadly applicable have been recently discussed.[10]

For larger systems, such as reactions involving biomolecules, mixed quantum mechanics/molecular mechanics (QM/MM) treatments have become popular.[11] In this approach the system is decomposed into a "reactive region" which is treated with a quantum chemical (or semiempirical) method whereas the environment is described by an empirical force field. This makes the investigation of certain processes feasible that would not be amenable to a full quantum treatment such that even free energy simulations in multiple dimensions can be carried out.[12] One of the current open questions concerns the size of the QM region required for converged results which was recently considered for Catechol O-Methyltransferase.[13]

The use of empirical force fields to follow chemical reactions dates back at least 50 years.[14–16] Such an approach has seen various incarnations, including the theory of diatomics in molecules,[14,15] empirical valence bond (EVB)[17] with its extension to several bonding patterns specifically for proton transport in water,[18] the ReaxFF force field,[19] the reactive molecular dynamics force field (RMDff) initially developed for polymers and based on the concept of bond order,,[20,21] or adiabatic reactive molecular dynamics (ARMD)[22,23] together with its multi-state variants.[24–26] There is a broad range of reviews on the subject of investigating chemical reactions based on established treatments[27] of the potential energy surfaces with applications in gas phase,[28,29] solution,[30,31] and enzymatic reaction[32–36] dynamics and the technology has also been extended to coarse-grained simulations.[37]

The present work focuses on more recent developments and applications of machine learning techniques applied to problems involving reactions in the gas phase, in solution, and in enzymes. Most problems concerning the *representation* of the underlying potential energy surfaces are excluded, as these are already well covered by accompanying contributions to this special issue.[7,8] Rather, the present work focuses on the application of ML-based techniques to problems that can not otherwise be exhaustively sampled, on the interplay

between experimental observables and computations and how to exploit this for improved understanding of intermolecular interactions, and on dealing with entire reaction networks.

Machine Learning (ML) is a data-driven method based on statistical learning theory to generate numerical models that generalize to new data, not used in the learning process.[38] Ideally, ML models interpolate and extrapolate to new data but in general this needs to be verified for every task. Historically, ML can be traced back to work on "Turing's Learning Machine". In 1951 the "Stochastic Neural Analog Reinforcement Calculator" (SNARC) was built by Minsky and Edmonds as a summer research project which is considered one of the first "artificial neural network" (ANN). Limitations of the learning capabilities of ANNs were described in "Perceptron"[39] and convolutional (CNN)[40] and recurrent (RNN)[41] NNs were developed subsequently. In the 1970s automatic differentiation was developed[42] which eventually lead to backpropagation that allows to learn internal representations[43] and was first applied to NNs in the behavioural sciences.[44] With the possibility to compute extensive reference data sets, application of ML-based techniques to questions of chemical reactivity has become a powerful complement to established methods.

One aspect of particular interest in the present work concerns the interplay between observation and information obtained from a computer model. "Observation" in the present context can either be an experimental observation or one from another computation. As an example, the PES can be a parametrized or non-parametric representation of *ab initio* computed energies and the observables can be obtained from either a classical, quasiclassical or quantum nuclear dynamics simulation such as an inelastic scattering cross section. Conversely, it is also possible to start with a set of experimental observations, for example reaction rates, and aim at determining the corresponding underlying PES that supports these experimental observables.

2 Machine Learning of Reaction Observables

Machine Learning techniques can be used to develop comprehensive models for observables that are directly related to experiments. Examples include prediction of thermal[45–47] or quantum reaction rates,[47] state-to-state cross sections,[48] mapping initial to final state distributions,[49] or even chemical reaction yields.[50]

2.1 Learning Reaction Rates

Chemical reactions involve bond-breaking and bond-formation processes. Hence, if the explicit nuclear dynamics describing the transition between reactant and one or several possible products is of interest, the motion between the two involves transgressing a barrier on the multidimensional PES. Empirical force fields, originally based on experimental information such as structure, spectroscopy and thermodynamics[51–54] are not suitable for following chemical reactions as the bonding pattern between the atoms is fixed. With the advent of efficient electronic structure methods, attention has shifted to either complement existing parametrizations with information from (high-level) electronic structure data[6,55–59] or to develop models that are entirely based on quantum chemical calculations.[60]

From a microscopic perspective suitable methods to follow chemical transformations - e.g. quasi classical trajectory or quantum simulations - at a molecular length scale are sensitive to the *entire* PES and require a global, reactive PES. Representing such a PES can be very challenging even for triatomic systems[61,62] because their topographies can be rather complex.[63] An example for such a PES for the [CNO] reactive system is reported in Figure 1. These 3-dimensional PESs were represented as a reproducing kernel Hilbert space which exactly matches the reference *ab initio* calculations on the reference points.[64,65] Finding parametrized functions with similar performance is in general very challenging. An alterna-

tive are permutationally invariant polynomials.[66]

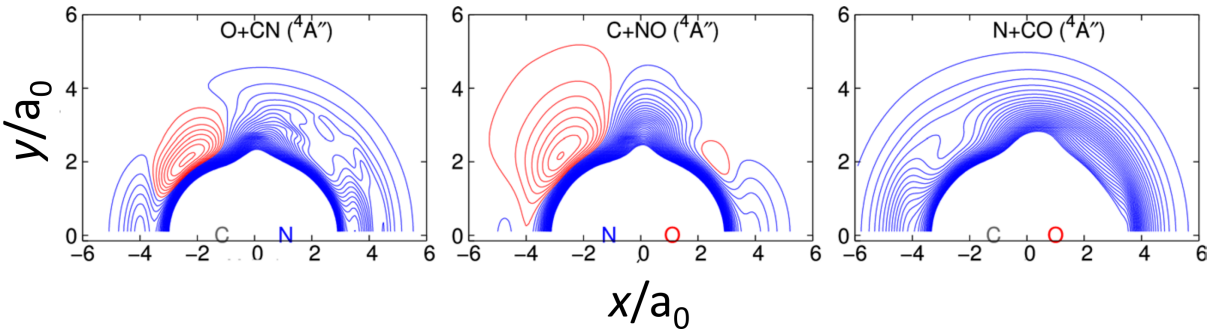


Figure 1: Contour plots of the ^{4}A" PESs for the [CNO] system represented as a reproducing kernel Hilbert space.[64,65] The diatoms (CN, NO, CO from left to right) are at their equilibrium structures (2.234, 2.192 and 2.150 a_0, respectively). The spacing between the isocontours is 0.2 eV with red lines corresponding to negative energies (–0.1, –0.3, –0.5 eV and lower) and blue lines to positive energies (0.1, 0.3, 0.5 eV and higher).

The determination of accurate reaction rates from computations is a formidable task even for seemingly simple A+BC→AB+C atom exchange reactions[62] such as the O+CN→[C+NO,N+CO] reaction for which PESs are illustrated in Figure 1. Modern approaches for gas phase reactions are based on a) the computation of thousands of energies at a high level of quantum chemical theory (e.g. coupled cluster (CCSD(T)) or multi reference (MRCI) treatments) using large basis sets, b) the representation of these energies either as a parametrized function[66] or using machine learning techniques such as neural networks,[7,67–70] reproducing kernel Hilbert space methods,[64,65,71,72] and c) following the nuclear dynamics either using classical mechanics (quasiclassical trajectory calculations (QCT))[16,73] or solving the three-dimensional nuclear Schrödinger equation. Such an approach is overall very computationally demanding and the quality of the computed rates depends sensitively on the accuracy of the underlying PES.[74]

In an effort to alleviate this problem, a recent effort[45] explored the possibility to use Gaussian

Process (GP) regression to train a correction $\chi(T)$ to predict thermal rates $k(T)$ in

$$k(T) = [\kappa_{\mathrm{ECK}}(T) k^{\mathrm{TST}}(T)] \chi(T) \tag{1}$$

Here, $k(T)$ was determined for ~ 50 different reactions based primarily on collinear collisions - which is a simplification but does not limit the general applicability of the approach - and the rates $\kappa_{\mathrm{ECK}}(T)$ and $k^{\mathrm{TST}}(T)$ are those from a simplified treatment of the Eckart tunneling correction (ECK) to conventional transition state theory (TST). Training was done for 13 reactions and the model was tested on 40 reactions. Between 3 and 5 descriptors were chosen to represent $\chi(T)$ and it was reported that judicious choice of the descriptors can lead to marked improvements in the model performance.

Compared with either TST or the Eckart treatment, the machine learned model performed best on the training set, on systems with symmetrical and asymmetrical barriers. In all cases, the error of the learned model ranged from 10 % to 120 % when compared with the exact data. This is a marked improvement over errors ranging from 80 % to 180 % (for ECK) and 180 % to 760 % (for TST). For reactions involving hydrogen abstraction from CH_4 the Eckart model was best, followed by the GP-trained model and TST. This study also highlights a critical need for both, the quality and quantity of reliable reference data in training such models. One surprising finding is the fact that using a model trained on collinear reactions ("2d") but applying is to a data set for reactions in full dimensionality ("3d") can perform quite well.

A recent application of this model concerned the $O(^3P)$+HCl→OH+Cl reaction[46] which can be considered as a particularly challenging example due to the large reaction barrier, the presence of low-energy reactive resonances and the heavy-light-heavy character of the system. Future applications of such an approach may be possible on sufficiently extensive and

curated data sets from actual experiments. As the reference data originated from a broad range of PESs it would also be of interest to determine whether model prediction can be further improved if all PESs are based on the same or a similar level of theory.

Machine learning approaches were also extended to one-dimensional quantum reaction rates.[47] Based on a large number of quantum rates $k_{\mathrm{Q}}(T)$, a deep neural network (DNN) was trained. The potential energy surfaces considered include single and double barriers, symmetric and asymmetric shapes. The optimized DNN, trained on $\sim$ 1.5 million data points, was then applied to predicted rates for a range of gas phase and surface reactions. The overall accuracy on the test set for $\log k_{\mathrm{Q}}(T)$ was 1.1 % and even at temperatures below 300 K for which tunneling effects ae expected to become important, the relative error was only $\sim$ 30 %.

2.2 State-to-State Models and Rates

Maintaining the full dimensionality of the problem, a NN-based, machine learned model was developed for the state-to-state (STS) cross sections of the $\mathrm{N}(^4\mathrm{S})+\mathrm{NO}(^2\Pi) \rightarrow \mathrm{O}(^3\mathrm{P})+\mathrm{N}_2(\mathrm{X}^1\Sigma_g^+)$ reaction.[48] These reactions are relevant in the atmosphere and for hypersonic flight.[75] For the ^{3}A' state the total state space for this problem, i.e. the total number of state-to-state transitions, involves a maximum of 47 and 57 vibrational states for NO and N_2, respectively, and maximum rotational quantum numbers for NO and N_2 of 241 and 273. Hence, there are 6329 ro-vibrational states for the N+NO channel, and 8733 states for the O+N_2 channel. To converge one specific state-to-state cross section $\sigma_{v,j\rightarrow v'j'}(E_t)$ for given translational energy E_t typically 10^4 to 10^5 QCT simulations need to be run. Doing this for the 10^4 initial states going into all 10^4 final states would require an estimated 10^{12} to 10^{13} QCT trajectories for directly sampling all available ro-vibrational states which is computationally impractical, even for this low-dimensional 3-body system. For diatom-diatom collisions the number of transitions increases to $\sim 10^{15}$ and the necessary number of QCT simulations approaches

10^{20}.[76] In such situations, ML approaches can provide an alternative to address the problem of characterizing product distributions from given reactant state distributions or more generally to determine final distributions from initial distributions given specific evolution equations or rules. In previous work,[48] a model for state-to-state (STS) cross sections from quasi classical trajectory (QCT) simulations of an atom-diatom collision system using a neural network (NN) has been proposed.

State-to-State Model The NN architecture for this application was based on ResNet[77] which uses identity shortcut connections to alleviate the vanishing gradient problem[78] that slows down the learning capacity with increasing depth of the NN. The input is transformed through four identical residual blocks,[77] after which a linear transformation followed by a scaled sigmoid function is used to project onto the final output.[48] The weight matrices $\mathbf{W} \in \mathbb{R}^{F\times F}$ (weight matrix) and $\mathbf{b} \in \mathbb{R}^{F}$ (bias vector) contain the parameters to be optimized. The residual blocks consist of two dense layers with the same number of nodes (here $F = 24$) and transform their input $\mathbf{x}^l$ according to

$$\mathbf{x}^{l+2} = \mathbf{x}^l + \mathrm{ReLU}[\mathbf{W}^{l+1}\mathrm{snasinh}(\mathbf{W}^l\mathbf{x}^l + \mathbf{b}^l) + \mathbf{b}^{l+1}], \tag{2}$$

The superscript l labels parameters for layer l. Two different activation functions, one for rectified linear units (ReLU)[79] and a self-normalizing[80] inverse hyperbolic sine (snasinh)[81] are used in the residual blocks. The final output is obtained from

$$y = C \times \mathrm{sig}(\mathbf{W}^o\mathbf{x}^l + b^o), \tag{3}$$

where $C = 0.4$ is a scaling constant, $\mathrm{sig}(x) = (1 + e^{-x})^{-1}$ denotes the sigmoid function and the superscripts o and l denote parameters $\mathbf{W}^o \in \mathbb{R}^{F\times 1}$ and $b^o \in \mathbb{R}$ corresponding to the output layer and the hidden features $\mathbf{x}^l$ obtained after the last residual block, respectively.

The 12 input features **f** are (i) internal energy, (ii) vibrational energy, (iii) vibrational quantum number, (iv) rotational energy, (v) rotational quantum number, (vi) angular momentum of the diatom, (vii) relative translational energy, (viii) relative velocity, (ix, x) turning periods of the diatom, (xi) rotational barrier height and (xii) vibrational time period of the diatom. For state-to-state cross sections, the same 12 features for the final states of the products are also included as input (i.e., $N_{\text{in}} = 24$). The loss functions (L_f) was

$$L_f = \frac{1}{N}\sum_{1}^{N}[\log(y' + 1.0) - \log(y' + |y - y'| + 1.0)]^2, \tag{4}$$

where y' and y are the reference (QCT) and predicted values (NN), respectively. All parameters of the NN are initialized according to the Glorot initialization scheme[78] and optimized using Adam optimization.[82]

To quantify the accuracy of the NN, additional QCT calculations were performed for independent initial conditions at fixed E_t. Total QCT cross sections are then compared with the NN predictions, see Figure 2. Again, the NN results describe the explicit QCT simulations which validates the use of such a model to predict microscopic information for such a reaction.

Initial state specific rates for the reaction were also calculated at temperatures between 2000 and 20000 K for a few selected reactant states using QCT simulations and compared with the rates obtained from the NN models. The NN models successfully capture the rates from QCT, see Figure 3. Although maximum relative errors of $\sim 17\%$ are found for specific initial states, in most cases the relative errors are $< 5\%$. State-specific and total reaction rates as a function of temperature from the NN are in quantitative agreement with explicit QCT simulations and confirm earlier simulations and the final state distributions of the vibrational and rotational energies agree as well.

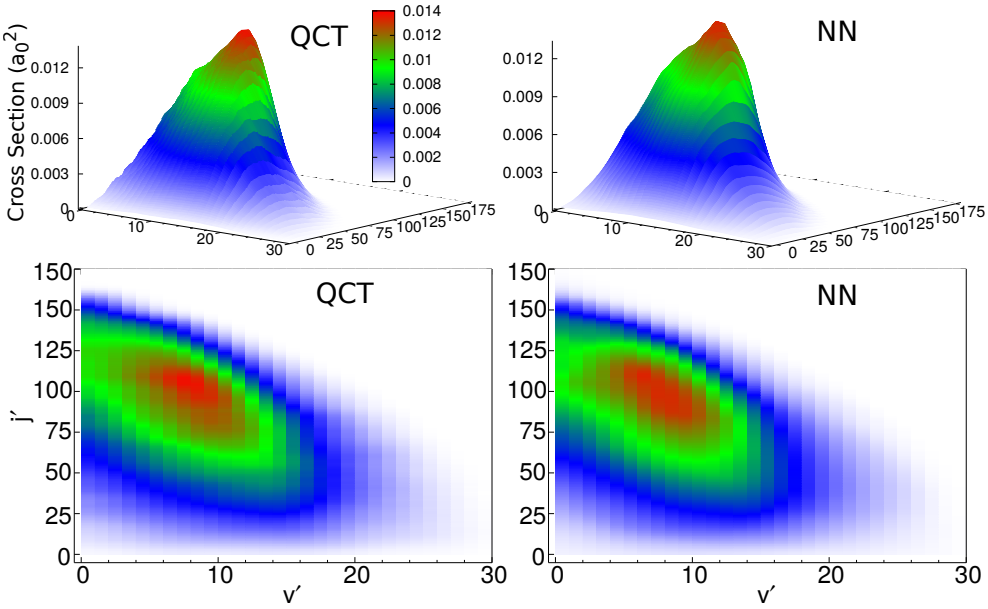


Figure 2: 3D surface (upper panel) and contour color map (lower panel) of QCT calculated and NN-STS predicted state-to-state cross sections for N + NO($v = 6, j = 30$) → O + $N_2(v', j')$ at $E_t = 2.5$ eV.

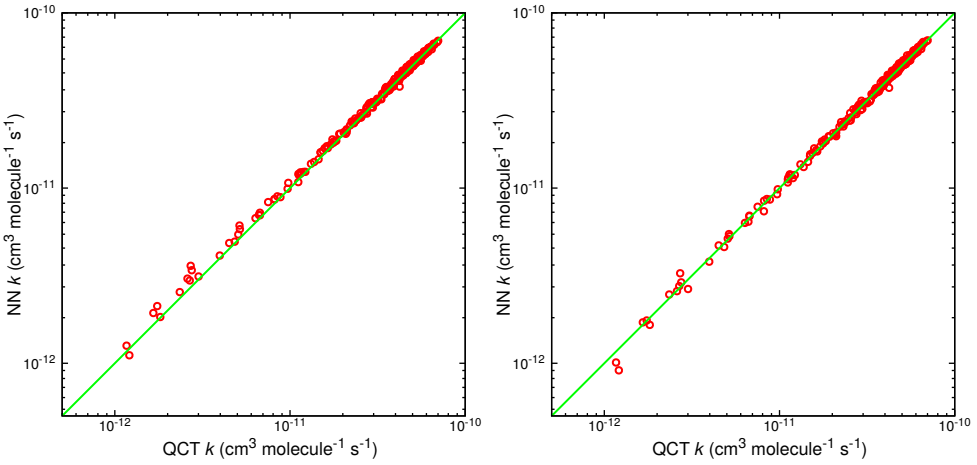


Figure 3: Correlation between the QCT-calculated and NN-predicted initial state selected rates. Left panel: Initial state selected QCT vs NN-STS rates for $v = 5, 10, 15$ and 20, $j = 20, 25$, 40, 60, 85 and 110, and at $T = 2000$, 4000, 6000, 8000, 10000, 12000, 14000, 16000 and 18000 K. Right panel: Total QCT vs NN-Tot rates at $T = 1000$, 2000, 3000, 4000, 5000, 8000, 10000, 12000, 15000, 18000 and 20000 K. Diagonals are shown as solid lines.

Distribution-to-Distribution Model In a recent extension, the STS model was generalized to a distribution-to-distribution model[49] for the relative translational energy E_{trans}, the vibrational v and rotational j states of a reactive atom-diatom collision system. Hence the NN-based model trained involved the reactant state distributions ($P(E_{\text{trans}}), P(v), P(j)$ where (v, j) labels the rovibrational state of the diatom) and predicts the three corresponding product state distributions ($P(E'_{\text{trans}}), P(v'), P(j')$) whereby $P(v)$ and $P(j)$ are marginal distributions, i.e. $P(v) = \sum_j P(v, j)$ and $P(j) = \sum_v P(v, j)$. Working with the underlying distributions leads to considerably smaller NNs that need to be trained which also speeds up the learning process. For this task, a multilayer perceptron with two hidden layers was used with 10 to 40 input and output nodes depending on the representation of the distributions. The two hidden layers contain between 6 and 12 nodes each.

For representing the distributions, parametrized functions (F), ML-representations based on reproducing kernels (K), and the actual grid points (G) were considered. In general, all three approaches accurately describe the (equilibrium Boltzmann) reactant state distributions. However, the product states are nonequilibrium distributions as they are from high-temperature simulations, ranging from 2000 K to 20000 K. Figure 4 reports final translational and vibrational distributions $P(E'_{\text{trans}})$ and $P(v')$ from different simulations compared with the machine learned predictions. For Figures 4A and B the QCT simulations were from conditions representative of the average R^2 over all test data for the respective method, i.e. using F-, K-, or G-based representations of the distributions. For conditions most representative of the average performance, a function-based approach is somewhat better suited ($R^2 = 0.999$) than a K-based ($R^2 = 0.998$) or a G-based ($R^2 = 0.999$) approach.

The representation by fitting to parametrized functions (F-based) leads to differences, in particular for $P(v')$ (e.g., deviations for small and high v' or extra undulations in Figure 4C. However, the deviations observed for high v' are only partially relevant, as the accessible

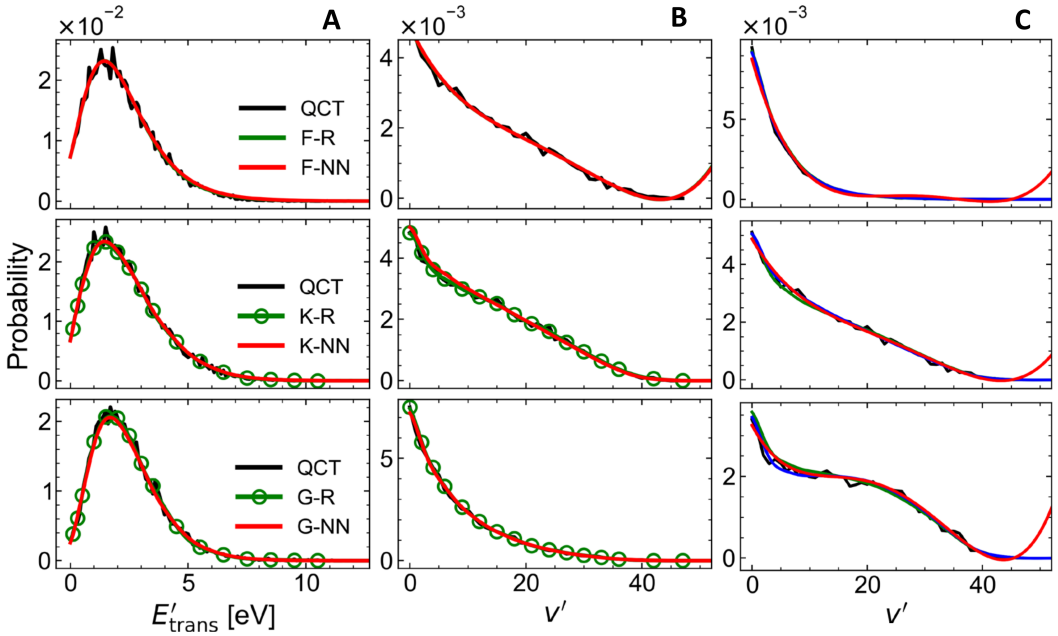


Figure 4: Product state distributions from explicit QCT simulations (QCT, black traces) as well as the corresponding reference data (-R) and the predictions (-NN) from the F-based (top), K-based (middle) and G-based (bottom) approaches. Also, the amplitudes to construct the reference RKHS-based representations in the K- and G-based approaches are reported (circles). For panels A and B the data sets are from QCT simulations with initial conditions sampled at translational, vibrational, and rotational temperatures ($T_{\mathrm{trans}}, T_{\mathrm{vib}}, and T_{\mathrm{rot}}$) for models representative of the average performance of the NN for each of the representations. These temperatures are (9500 K, 16000 K, 16000 K), (10250 K, 19250 K, 19250 K), and (12000 K, 9750 K, 9750 K) and [$\mathrm{RMSD}_{\mathrm{NN}} = 0.0005$, $R^2_{\mathrm{NN}} = 0.9995$], [$\mathrm{RMSD}_{\mathrm{NN}} = 0.0013$, $R^2_{\mathrm{NN}} = 0.9984$], and [$\mathrm{RMSD}_{\mathrm{NN}} = 0.0009$, $R^2_{\mathrm{NN}} = 0.9993$] for F-, K-, and G-based representations, respectively. In panel C the final vibrational distributions are reported for initial conditions at temperatures (12500 K, 5750 K, 5750 K), (9500 K, 16000 K, 16000 K), and (5750 K, 19250 K, 19250 K) for the top, middle, and bottom panels. Towards the highest values v' the F-based approach (red) is unable to correctly model $P(v')$. Note also the stark contrast to a typical Boltzmann distribution for the vibrational state distribution for the middle and bottom panels in C. Figure adapted from Ref. [49]

vibrational and rotational state space is finite, here $v'_{\mathrm{max}} = 47$, $j'_{\mathrm{max}} = 240$. Considering the K- and G-based approaches, the reference representations describing product distributions are nearly identical and reproduce the QCT data very closely, see blue and green traces in Figure 4C.

2.3 Gaussian Processes and Bayesian Inference

Gaussian Process (GP) regression is a non-parametric, supervised learning technique and one of several kernel-based methods to generate ML models.[83] Previously, GP has been applied to regression and classification problems but more recently it has also been used to represent intermolecular PESs[61,84] and, combined with Bayesian optimization, to address the inverse problem of reactive scattering.[85] The "inverse problem" of determining the interaction potential from scattering data is a long-standing problem in chemical physics[86–90] and has been handled within Tikhonov regularization and using minimization procedures for diatomic molecules.[91]

The problem has been formulated in a combined GP and Bayesian inference context.[92] The formal development starts from a global, reactive PES expressed as $V(\vec{r}) = \sum_{i=1}^{N} w_i(\vec{r})E_i$, similar to MS-ARMD,[24] where E_i are energies from an *ab initio* calculation and the weights $w_i(\vec{r})$ are optimized through GP regression to yield most accurate scattering cross sections. A GP is entirely specified by the conditional mean $\mu(\vec{r}_i)$ and the conditional variances $\sigma(\vec{r}_0)$ at an arbitrary configuration $\vec{r}_0$. The conditional mean and variances can be represented as an $n-$dimensional vector and a $n \times n$ square matrix of covariances, respectively.[85] The GP model is trained by determining the best covariance matrix given a set of reference data (e.g. energies from *ab initio* calculations or scattering cross sections). In order to progress, a model for the covariances needs to be assumed which can be Matern functions, Gaussians, rational quadratic kernels or other simple functions.[83] The model is then optimized using a suitable likelihood function which is the log marginal likelihood as is customary for GP optimization. It is noted that up to this point such an approach is also reminiscent of the reproducing kernel Hilbert space technique which employs different classes of functions for representing the kernel matrix and which has been successfully used to represent PESs.[64,65,71,72,93–103]

To make an inference (prediction) of an unknown value y_* at a given value $\vec{r}_*$ one can use

Bayes' theorem according to which

$$P(y_*|\vec{y}) = \int_\theta P(y_*|\theta)P(\theta|\vec{y})d\theta \tag{5}$$

where θ is a vector containing the model parameters and $\vec{y}$ are the known values (e.g. energies from *ab initio* calculations or scattering cross sections).[85] If the model parameters θ are not fixed but random variables themselves, a Bayesian NN is obtained. More specifically, if Gaussian distributions are assumed for the parameters and in the limes of an infinite number of neurons, the Bayesian NN has been shown to map onto a GP.[85]

This formalism has been recently applied to reactive scattering for the H+H_2→H_2+H and the OH+H_2→H_2O+H reactions. It was reported that for the H+H_2→H_2+H reaction with as few as 37 points (taken from a total of 8701 reference energies from which a global PES had been fitted previously) accurate reaction probabilities can be obtained.[92] Similarly, for the more challenging OH+H_2→H_2O+H reaction 290 points from a total of $\sim$ 17000 *ab initio* energies were sufficient to cover the entire 6-dimensional PES to obtain accurate reaction probabilities as a function of the translational energy of the reactants.[92]

It is worthwhile to mention that with increasing dimensionality GP-based representations become computationally expensive.[74] On the other hand, increasing the kernel complexity, e.g. by using composite kernels, both the performance[104,105] and accuracy[106,107] of this approach have been found to improve.

3 Reaction Rates and Pathways

Reaction rates can be determined from classical or quantum dynamics simulations if suitable PESs are available that allow bond formation and bond breaking. Ideally, such PESs are

global, i.e. they allow - starting from a reactant structure - to form all chemically meaningful and energetically accessible product states. In practice, generating such global PESs is extremely challenging[29,108] or even impossible due to the large number of reaction pathways. The global nature of the PES is particularly important in high-energy processes such as hypersonics or in combustion. While for hypersonics[62,75,109–113] the relevant species are often atoms and diatomics, this is not the case for combustion[2] or for atmospheric and astrophysically relevant[1,3,114,115] processes for which the species involved can be larger and the number of possible product channels therefore increases considerably.

To illustrate the problem for following a chemical reaction of an atmospherically relevant molecule isomerization and decomposition pathways for acetaldehyde (AA) are considered. These processes are relevant for atmospheric chemistry because it has been proposed that formic acid (FA) can be generated via oxidation by the hydroxyl radical[116,117] following photo-tautomerization of AA to its enol form VA.[118–120] Pathways in addition to the conventional route (photochemical oxidation of biogenic and anthropogenic volatile organic compounds (VOCs)) for formation of FA are required to account for the global budget of formic acid.[121]

To characterize the isomerization between AA and VA under conditions relevant to the atmosphere a NN-based, reactive PES was constructed[122] based on PhysNet.[69] Such a PES is required to run statistically significant numbers of trajectories based on QCT simulations[24,123] because ab initio MD simulations are computationally too expensive. The excitation energy in the simulations was 93.6 kcal/mol which compares with energies of 86.6 kcal/mol to 95.3 kcal/mol for actinic photons. At this excitation energy no isomerization reaction from AA to VA was observed but decomposition into CH_4+CO, and H_2+H_2C_2O occurred. It was found that for an accurate representation of all states involved (AA, VA, CH_4+CO, and H_2+H_2C_2O) and for stable NVE simulations more than 4×10^5 reference energies at the

MP2 level of theory with an aug-cc-pVTZ basis set were required.[122] For energies up to 93.6 kcal/mol (isomerization barrier between AA and VA at 68 kcal/mol and excitation energy by actinic photons) the MAE and RMSE are 0.0071 kcal/mol and 0.0145 kcal/mol, respectively. In order to validate that the NN-PES does allow isomerization, higher excitation energies up to 127.6 kcal/mol were used. The global PES has then a MAE and an RMSE of 0.0132 kcal/mol and 0.0307 kcal/mol, respectively.

These simulations found that for excitation energies of $\sim$ 95 kcal/mol - corresponding to actinic photons - not a single isomerisation occurred on the 500 ns time scale. Hence, formation of FA following electronic excitation with actinic photons of AA and subsequent ground state relaxation and isomerisation to VA (and/or further chemical processing) appear unlikely to occur, in contrast to the interpretation of the experiments.[116] Rather, after photoexcitation of AA the system either decomposes or relaxes through internal vibrational energy distribution.

Another ML-based approach that was recently followed to construct reactive PESs and use them in dynamics simulations is based on permutationally invariant polynomials (PIP)[66,124] combined with a neural network (PIP-NN).[125] For conventional PIP, the expansion coefficients in the polynomials (usually in Morse-variables) are fitted using a linear least squares algorithm whereas for PIP-NN the coefficients are trained by a NN. PIP-NN has been applied to both, gas-phase and surface reactions.

In the gas phase, PIP-NN has been applied[126] to reactions such as HO+CO$\rightarrow$H+CO_2 which is relevant in the atmosphere and in combustion.[127] A total of $\sim$ 75000 was used to represent this channel. The PES was used in QCT and quantum dynamics simulations to determine total reaction probabilities, thermal rates, differential cross sections, and product state vibrational and rotational distributions[126] as well as tunneling probabilities and survival fractions.[128] Comparison between a pure NN, a pure PIP, and the PIP-NN approaches

demonstrates that despite the rather small differences in the fitting quality certain observables, such as product state distributions or differential cross sections can sensitively depend on the shape of the PES.

PIP-NN has also been used for reactive scattering involving metal surfaces. Systems investigated include H_2/Ag(111),[129] H_2/Co(0001),[130] H_2O/Ni(111),[131] and CO_2/Ni(100).[132] The number of reference points in these applications ranged from several 1000 to $\sim$ 25000. For the dissociative chemisorption of water on rigid Ni(111), QCT simulations using a nine-dimensional PIP-NN PES fitted to energies from density functional theory it was found that the reactivity depends on the impact sites and the incident angle of the water molecule.[131] Furthermore, analysis of the simulations demonstrated that both, the barrier height and the topography of the PES influence the reaction rate as does the translational energy both, parallel and perpendicular to the surface.

More recently, PIP-NN has also been extended to larger systems, including the F+ $CH_3OH \rightarrow$ HF+CH_3O reaction[133] or the investigation of the Cl+$CH_3OH \rightarrow$HCl+ CH_3O/CH_2OH reaction.[134] These examples illustrate that it is possible to follow reactions with multiple product states in a realistic fashion. For instance, the HCl vibrational and rotational product distributions and the product translational energy distributions compare well with experiment.

Complementary to reactions with multiple reaction products, multiple step reactions with one or several intermediates between reactant and product pose another challenge. A recent application concerned the thermal activation of methane by MgO^+ for which experimental rates were determined between 300 K and 600 K.[135] Another example is the unimolecular decomposition of the CH_3COOH Criegee intermediate.[136] Recent simulations based on an MS-ARMD and NN-trained full-dimensional energy surface involving the reactant, H-transferred intermediate, and OH-elimination product (see Figure 5 demonstrate that stepwise reactions

can also be followed by such techniques. Figure 5 demonstrates that empirical FFs can be fit with an accuracy of $\sim$ 1 kcal/mol ("chemical accuracy") whereas using PhysNet to train the same data reaches an accuracy of 0.02 kcal/mol. The preliminary rates from MD simulations are consistent with experimental values.

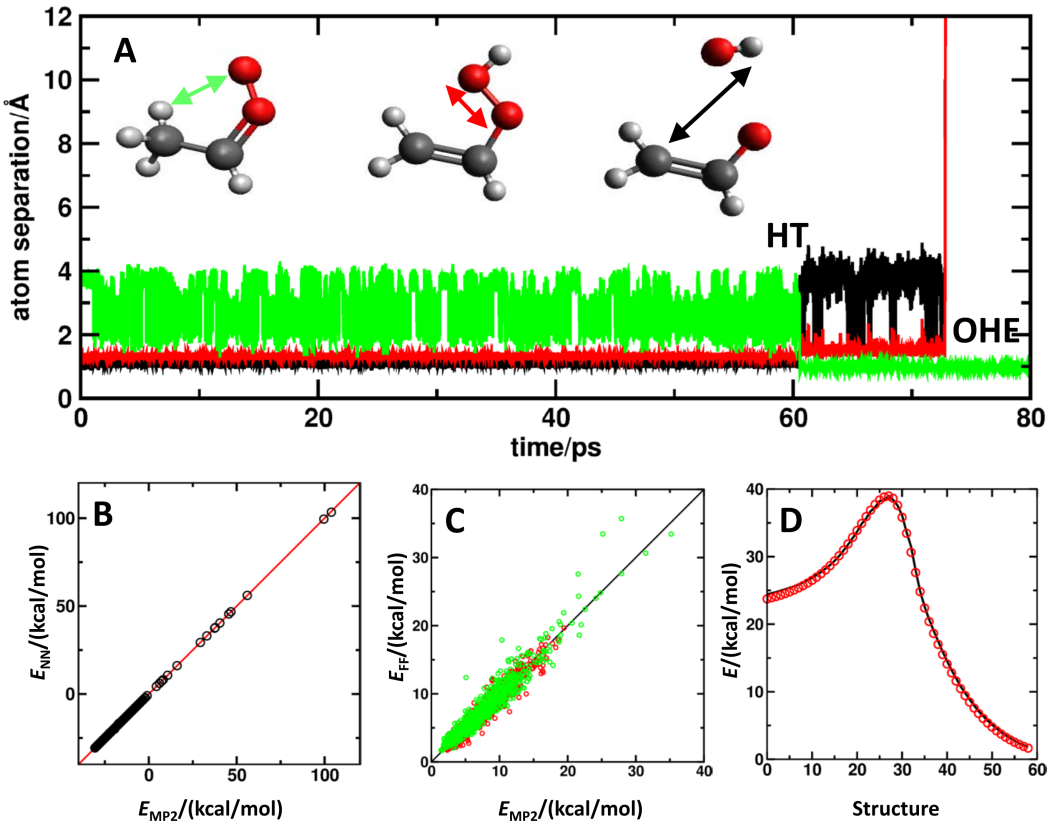


Figure 5: Stepwise reactions for the Criegee intermediate. Panel A: Time dependence of important atom separations, the CH (black), OO (red), and OH (green), for the H-transfer (HT) and OH-elimination (OHE) reaction. Panel B: PhysNet[69] model for $\sim 10^5$ MP2 reference energies together with the correlation between them (red). Panel C: MS-ARMD[24] model for $\sim$ 100 reference structures for reactant (red) and product (green) structures. The RMSD is $\sim$ 1 kcal/mol and the 1 : 1 correlation is the black line. Note the different energy scales in panels B and C. Panel D: minimum energy path for H-transfer between reference (red circles) and MS-ARMD fit (black). Energy-dependent rates from both models for the energy (PhysNet and MS-ARMD) are in good agreement with experiment.[137]

It should be emphasised that despite the undoubted accuracy of the reactive PESs discussed above and their utility for interpreting experiments and further elucidate the reaction dynamics of the systems, they are not truly "global" PESs. Typically, the research decides what

channels are considered or of interest and the corresponding breakup channels are included in the ML-based construction of the interpolant. Thus, for systems with more degrees of freedom and a larger number of product channels it is possible that important states are omitted despite the powerful methods available for (re)constructing the underlying PESs. If omitted, such channels will fundamentally affect the resulting reaction network and the realism with which one is able to map it to a computational model and provide a meaningful complement to experiment.

4 ML Applications to Reactive Biological Systems

4.1 Reactive Molecular Dynamics for Ligand Binding to Proteins

Proteins are too large and the time scales of bond-breaking and bond-forming reactions too long to be amenable to full *ab initio* MD simulations. Hence, mixed QM/MM simulations which decompose the system into a (small) reactive subsystem treated with quantum mechanical methods and an environment described at the level of an empirical force field are one of the methods of choice.[10,11] Alternatively, methods such as the empirical valence bond (EVB) theory,[17,32] or multi state adiabatic reactive MD[24] have been developed and applied. More recently, ML-based energy functions such as reproducing kernels (RKHSs) have been used to follow bond-breaking and bond-formation in biological systems. One example is nitric oxide binding to myoglobin (Mb).[100] For this, a 3-dimensional RKHS PES was fitted to reference density functional theory calculations for radial and angular degrees of freedom of the NO ligand with respect to the heme unit and the iron out-of-plane motion with respect to the heme plane. All remaining degrees of freedom of the solvated protein-ligand system were treated with an empirical energy function.

Extensive reactive MD simulations with such a mixed ML/empirical energy function pro-

vided the first structural interpretation of the metastable states in Mb-NO.[138] Consistent with recent optical and X-ray absorption experiments, which are unable to directly relate spectroscopic response with the underlying structure, these simulations found two processes: one on the 10 ps and another one on the 100 ps time scale. They correspond to rebinding of the ligand to Histidine64 in an "open" and a "closed" conformation. A mixed and reactive ML/empirical energy function paired with the accuracy of RKHS to represent the reference points is required to carry out the necessary statistical sampling and reach the time scale of the processes which is not possible with QM/MM techniques.

4.2 Computer-Guided Enzyme Design

Computer-based methods have also been used to modify or design amino acid sequences that catalyze organic reactions.[139] Although a comprehensive and generally accepted ML-based technology to do this is not available as of now, the recent success of ML[140] in winning the CASP14[141] clearly foreshadows that machine learning will play an eminent role in design of enzymatically active amino acid sequences. One of the deciding factors was the deeper search capabilities of a CNN together with the choice of objective function to be optimized which included distances between C_β atoms, backbone torsion angles, and the prevention of steric clashes.[140] Thus, a combination of "trainability" through availability of curated and sufficiently complete reference data, judicious choice of target information with respect to which optimization can be carried out, and architecture of the underlying NN are drivers for successful ML missions.

Directed evolution has been used experimentally to (re)design enzyme function.[142] Starting from an originally designed Kemp eliminase[143] the efficiency of the protein was assessed after 7 and 17 rounds of evolution and found to have increased by more than a 9 orders of magnitude. Analysis of nuclear magnetic resonance (NMR) measurements indicated that

the key difference between the original and the evolved enzyme are the dynamic fluctuations of the catalytic amino acids that increase the probability to occupy catalytically proficient conformation and reduce the number of overall possible conformations.[142] Given the inherent similarities of evolutionary strategies and neural networks it is expected that ML-based technologies will provide further scope to apply computer-based techniques for optimization and even reshaping protein sequences for particular reactions. Solving such problems is akin to the quest followed in materials design which aims at using ML to develop materials with given properties (such as electrical conductivity, melting point, or hardness).

5 Machine Learning in the Context of Experiments

Relevant experimental observables in the context of chemical reactivity can include characteristics as diverse as the prediction of reaction probabilities.,[45,46,85] differential cross sections or product state distributions,[48,62] the prediction of reaction outcomes (given specific input compounds),[144,145] finding optimal reaction conditions,[146,147] or predicting and identifying fragmentation patterns from mass spectroscopy.[148,149] For prediction of reaction outcomes it is worthwhile to mention that some of the efforts go back at least 50 years with initial efforts to use computer-aided strategies for organic synthesis (CAOS).[150–156] Similarly, using ML-based techniques (referred to as "AI" at the time) for analysis of mass spectrometric data started also in the mid-1960s with DENDRAL.[157–159]

5.1 Organic Reactions

The field of "retrosynthesis" started around 1967.[151] Since then, much progress has been made. Initially, rule-based expert systems such as CAMEO[156,160] or EROS[161] have attempted to predict reaction outcomes. It was found that such approaches do not scale well

and are not easily generalizable. Later attempts were based on machine learning approaches from training of labeled reactions.[162] The ReactionPredictor uses a feature vector consisting of physicochemical and topological features, including molecular weight, formal and partial charges of the atoms, information about atom sizes, together with information similar to molecular fingerprints. For training the network, 1516 features were retained. The learning was done within an artificial NN with sigmoidal activation functions and one hidden layer, i.e. a shallow NN. For organic textbook reactions as the training and the validation set $\sim$ 96 % accuracy was reported.[162] Using a fingerprint-based NN an accuracy of 80% of selected textbook reactions was found.[144] The main limitation in this prediction exercise was due to the limitations of the SMARTS transformation to describe the mechanism of the reaction type completely. Due to the flexibility in the descriptor it is possible to further expand this algorithm to account for the reaction conditions.[144] Similarly, deep reinforcement learning has been applied to optimize chemical reactions.[146] For 4 different reactions it was shown that with the product yield as the objective to maximize the Deep Reaction Optimizer (DRO) found the optimal conditions within 40 steps, with the total time of 30 min required to optimize a reaction in a microdroplet. Also, optimizing reaction conditions for on one type of reaction and testing on a different reaction (here the Pomeranz-Fritsch synthesis of isoquinoline and the Friedländer synthesis of substituted quinoline, respectively) reached a higher yield with fewer optimization cycles.

Despite these achievements, there are still limitations in using ML methods to predict the outcome of diverse organic reaction.[163] As an example of the intrinsic difficulties faced one can consider the issue of "learning" in a conventional ML context. Every ML model learns from a finite number of training data, is tested on further independent data and then can be used to predict on unknown data.[7] Typically, the larger the size of the training data, the better the model. There are on the order of 10^7 reactions with more than $\sim 10^4$ different reaction types.[164] This leaves only 10^3 samples for every reaction which typically does

not include different solvents, reaction conditions, substitutions and other determinants that drive a chemical reaction. Hence, the statistics for "learning" still needs to be improved.

It will be of interest to see whether computer-assisted techniques can contribute to alleviate such problems. Given the unparalleled increase in computer efficiency, larger numbers of reactant, product and transition state structures can be quantitatively evaluated routinely. One example are the very large data sets employed to train NN for molecular energy functions. The ANI-1 data set contains 2×10^7 structures of organic molecules.[165] For a summary of existing databases, see Ref.[166] With such approaches it may be possible to more broadly assess structural, substitutional and electronic effects on chemical reactivity that undoubtedly are relevant for reaction outcomes. In addition, the effects of solvent need to be included. There has been recent progress in developing ML-based models for hydration and solvation free energies on compounds.[167–170] This, together with the advances in electronic structure theory may provide an avenue for further improvements of the models.

Recently, a modular robotic system for organic synthesis consisting of a Chemputer, a Chempiler and a scripting language (ChASM) was combined to drive four modules consisting of a reaction flask, a filtration station, a liquid-liquid separation module and a solvent evaporation module.[171] This system was used to automate the synthesis of compounds such as diphenhydramine hydrochloride, rufinamide, or sildenafil without human intervention.[171] Besides the attractive prospect to automate standard chemical procedures with the opportunity to discover new synthetic routes, such procedures also enhance the reproducibility of synthetic procedures. An alternative approach of a robotics-based platform driven by software uses From 12.5 million published single-step reactions which were translated into a total of 163,723 rules.[172] With this input a forward NN was trained to predict what rules are most likely applicable for the synthesis of a particular target molecule. The testing of the platform was done on 15 reactions of different complexity. It was concluded that such

robotic platforms coupled with curated data and powerful ML algorithms can relieve scientists from routine tasks so that they can rather focus on the more creative steps that lead to new ideas.[172]

Similar advances have been reported in the area of materials sciences by introducing the concept of autonomous experimentation[173,174] based on Phoenics[175] and its successor Gryffin.[176] Phoenics uses Bayesian neural networks to create a kernel-based surrogate model for the efficient optimization of chemical and material properties. Like other Bayesian optimization approaches, Phoenics balances the exploration and exploitation of parameter space to achieve sample-efficient experimental campaigns. Hence, such an approach also falls within the broader class of "model optimization problems" that are also used for reactive networks.[177]

For the design of novel, functional materials with specific, predefined properties, which - by definition - involve chemical reactions and transformations, the problem at hand is further exacerbated by the fact that the parameter space contains continuous (e.g. T or flow rates) and discrete (categorical) variables, such as the type of solvent, chemical substitutions or the catalysts used. Gryffin,[176] an extension of the Phoenics framework, allows to tackle such optimisation problems by taking advantage of recent ML advances that enabled the continuous relaxation of discrete variables.[178,179] This approach has been applied to the autonomous optimization of a stereoselective Suzuki-Miyaura coupling between a vinyl sulfonate and an arylboronic acid to selectively generate the E-product isomer in high yield.[180] Along similar lines, reaction yield predictions were recently learned based on natural language architectures using an encoder model and a regression layer. As an example, the average R^2 for the Suzuki-Miyaura reactions was ~ 0.8, similar to a model only trained on the Buchwald-Hartwig reactions. It was concluded that such models can perform equally well on different types of reactions and are robust with respect to the parameters and hyperparameters of the

model.[50]

5.2 Mass Spectrometry

Chemical structure determination using data from mass spectrometry was one of the early applications of expert systems ("AI") to problems involving decomposition reactions.[158] The earliest ML-based program to do this was "DENDRAL".[159] In a later effort,[181] the insights gained from reaction predictions using EROS[161] were used to develop a computational framework (MAss Spectra SIMulatOr - MASSIMO) to predict the mass spectrum given the structure of the compound. To put a criticism of DENDRAL into context ("..it is sad to say that, in the end, the DENDRAL project failed in its major objective of automatic structure elucidation by mass spectral data..")[181] it should be noted that DENDRAL was aimed at the reverse task: structure determination for given mass spectrometric data.

More recently, NN-based techniques were developed to address the problem of competitive fragmentation modeling for electron ionization (CFM-EI).[148,182] Given a chemical structure the model predicts an electron ionization (EI) mass spectrum (MS). Contrary to another approach available, CSI:FingerID,[183] competitive fragment modeling is applicable to both, ions generated from electron ionization as well as electrospray ionization (ESI). CFM-ESI uses a probabilistic model based on systematic removal of all bond connections, every pair of bonds in rings, and considering all hydrogen rearrangements within the resulting fragments. The chemical features required for training the NN include properties such as broken bond types (single, double, and others), neighboring bond types, functional group features,[184] and others.[148] The data set for training, testing and validation contained $\sim$ 20000 molecules. The performance of this model was 77 % when querying against the measured reference spectra and 43 % against the NIST database.

Compound structure identification (CSI) in predicting fingerprints and identifying metabolites (FingerID), referred to as CSI:FingerID,[183] uses molecular fragmentation trees with molecular fingerprint prediction based on multiple kernel learning.[185,186] Here, training was carried out on $\sim$ 6200 compounds. With the full training set the correct identification rate is $\sim$ 30 %.[183] In a comparative assay based on PubChem, the identification rate for CSI:FingerID was $\sim$ 32 % compared with $\sim$ 12 % for CFM-ID.[183]

Most recently, analysis of high-resolution fragmentation mass spectra was carried out based on "class assignment and ontology prediction using mass spectrometry" (CANOPUS).[149] This workflow employs a number of support vector machines (SVMs) to predict fingerprints of the query compound which is the input to a deep neural network to predict all possible compound classes consistent with the query compound simultaneously. The SVMs are trained on experimental reference mass spectrometric data. Conversely, the DNNs are trained on millions of compound structures with molecular formulae as the feature vectors together with the number of atoms of a given type, the mass, and additional atom-based features as input to the DNN.[149] The binary molecular fingerprint, determined from CSI:FingerID,[183] and the molecular formula features from a fragmentation tree[187] are used as input to the DNN. The DNN is optimized using Adam.[82] With respect to performance as measured by the Matthews correlation coefficient (MCC = +1 for perfect classification and MCC = −1 for a completely wrong classification)[188] the ranges are from 0.875 for steroids to 0.972 for phosphocholines from the training set. For the test set, the MCCs ranged from 0.60 to 0.74.[149]

6 Machine Learning for Entire Reaction Networks

Reaction networks are relevant in various branches of chemistry, including but not limited to atmospheric reactions, combustion, astrophysical and biological networks. Often such

networks are sampled at the level of a stochastic network[189] by solving a large number of coupled ordinary differential equations.

More recently, it was attempted to directly propagate the nuclear dynamics within an *ab initio* nanoreactor.[190] Such an approach is still rooted in conventional *ab initio* molecular dynamics simulations and limited to the level of theory employed and the time scales accessible to such simulations. Very recently, a NN-based model was presented to follow combustion reactions in space and time.[191] These simulations used the DeepMD NN architecture[192] to compute energies and forces for methane combustion (starting 100 CH_4 and 200 O_2 molecules) at 3000 K and found 798 different chemical reactions, some of which were as of now unknown.[191] The total simulation time covered was in the nanoseconds and the accuracy of these simulations is only limited by the electronic structure data the NN was trained to.

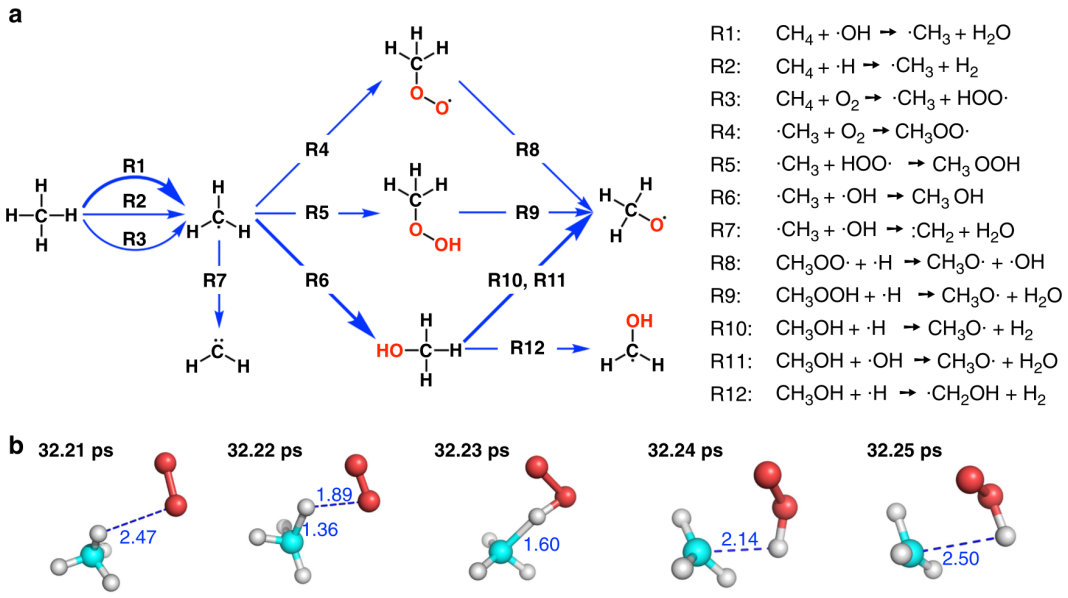


Figure 6: The initial stage of methane combustion. Panel a: Primary reaction pathways (left) and reactions R1 to R1 (right) during the initial stage of the combustion. Panel b: A real-time trajectory showing the reaction progress over 40 fs for hydrogen abstraction from methane by O_2. Carbon, oxygen and hydrogen atoms are in cyan, red, and gray, respectively, with atom separations reported in Å. Figure adapted with permission from Ref.[191]

In another recent attempt, methane combustion was simulated using an ML-trained model on atomization energies[193] using kernel ridge regression with a Smooth Overlap of Atomic Positions (SOAP) representation.[194] A mean-field, qualitative microkinetic simulation of a 50 : 50 mixture of CH_4 and O_2 using only the reaction energies (trained to an accuracy of $\sim$ 0.1 eV) and the law of mass action was carried out. The resulting reduced reaction networks as a function of abstract simulation time is reported in Figure 7. Several notable species are formed in this simulation, including methanol, formic acid, and Criegee intermediates.

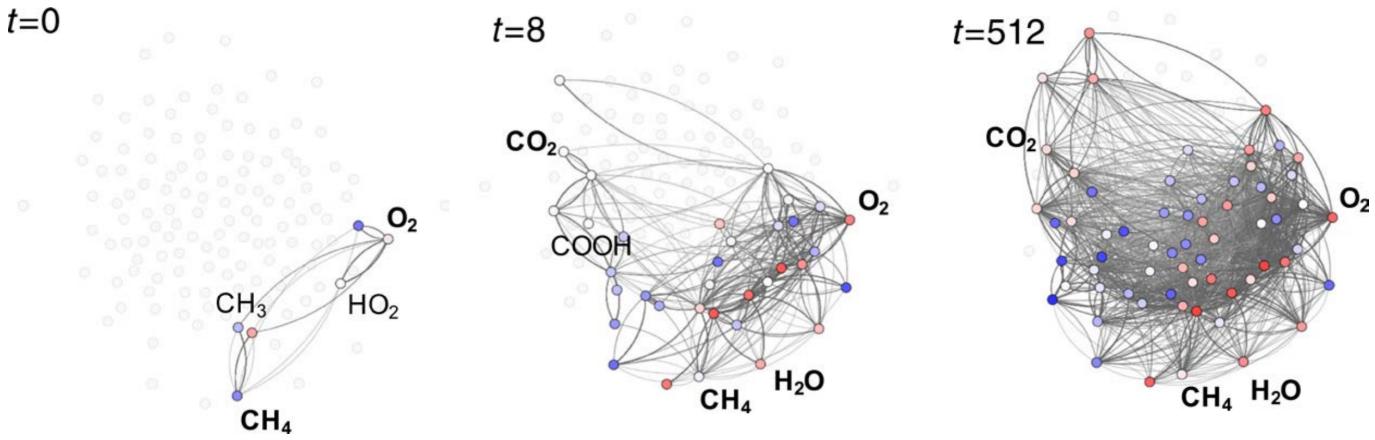


Figure 7: Methane combustion: each frame shows the reduced reaction network extracted from a microkinetic simulation of methane combustion depending on abstract, arbitrary simulation time. Reactants and products (bold) and intermediates (regular font) are indicated next to the nodes which are colored according to their absolute atomization energies from low (red) to high (blue). Figure adapted from Ref.[193] with permission.

Machine-learning investigations of entire chemical reaction networks were recently undertaken.[177] Using "automated learning of algebraic models for optimization" (ALAMO),[195] the "Reaction Identification and Parameter Estimation" (RIPE) tool was developed and used to estimate and identify kinetic rate parameters from a postulated superset of reactions. RIPE was applied to combustion reactors to model catalyst conversion, or alternative reaction mechanisms and stoichiometric relationships. Chemical looping combustion has been developed to isolate fuel from air in combustion reactions using an oxygen carrier shuttled

between two flow reactors. In this application the task solved by the ML approach is to select the model to best describe the input data from experiment. For the application to alternative reaction mechanisms the technique is used to discern between a large number of alternative mechanistic pathways. Such approaches fall under the general heading of "optimal model selection" given a concrete, preconceived reaction network. The RIPE tool is available from www.idaes.org and can handle between 10^2 and 10^4 reactions.

7 Future Developments

In the following possible developments in the field of ML-applications to chemical reactions are illustrated.

For small systems (containing few atoms) one question is whether in general the number of reference points for constructing global, reactive PESs can be dramatically reduced for accurate representations of intermolecular PESs when resorting to ML techniques. Previously, it was assumed that typically of the order of 10 points per degree of freedom is required for a good coverage of conformational space. Hence, for a diatom+diatom system of the order of 10^6 reference *ab initio* energies would be required. For global, reactive PESs this number is likely to be even larger. In the context of GP regression it has been argued that for an $N-$dimensional system only $\sim 10N$ well-selected points are required.[196] The work on combined ML and Bayesian optimization techniques[85] indicates that this is indeed possible for molecular systems, too. On the other hand, recent work on the SH+H→S(^{3}P)+H_2 reaction[61] estimated that rather 500 points are required for faithful representation of the global, reactive PES, contrary to the $\sim$ 30 points that were found to be sufficient for the H+H_2→H_2+H system[85] despite the same dimensionality. Hence, the number of points required may depend on the presence of (permutational) symmetry and the chemical species

involved and hence the overall topology of such a PES.

One of the challenges ahead in the field is to learn high-quality PESs while minimizing the number of reference points required. It has been recently demonstrated that for high-dimensional, non-reactive systems a few hundred points are sufficient to accurately represent the near-equilibrium PES using RKHS representation on energies and forces.[103] For the two largest molecules (CH_3CONH_2 and CH_3COCH_3) 2500 reference energies were found to be sufficient to obtain a mean averaged error of 0.01 and 0.07 kcal/mol on 1000 test points. The harmonic frequencies determined from such PESs are typically within 1 cm^{-1} of a normal mode calculation using conventional normal mode analysis from quantum chemical calculations at the same level of theory with a maximum deviation smaller than 10 cm^{-1}.

Another relevant question concerns the probing and specific improvement of high quality PESs in view of experimental observables. The question that arises in this context is which parts of the PES are "reliable" and which parts can be further improved. Chemical reactions by their very nature are sensitive to the global shape of a PES whereas other observables such as harmonic frequencies only probe the local shape and couplings between degrees of freedom. The PES regions sampled for specific observables has, e.g., been reported for the $N(^4S) + O_2(X^3\Sigma_g^-) \leftrightarrow O(^3P) + NO(X^2\Pi)$ reaction.[197] Another study developed a Bayesian ML approach to quantify uncertainties on PESs for the reactive O_2+O system considering two different electronic states.[74] This effort started from Bayesian-based sensitivity analysis of computer models using GP.[198] Sensitivity analysis of PESs dates back at least 30 years[199] where the problem of inversion of ro-vibrational spectra for diatomic molecules has already been formulated within a Tikhonov regularization framework.

When using experimental observables to refine *ab initio* calculated PESs for Ne-HF it has already been found that specific observables are only sensitive to particular regions of the

PES.[200,201] Such "PES morphing approaches" have been extensively applied to small molecular systems.[202–218] There is also scope for extending this more broadly[26] and in the context of machine learned PESs, as has been recently indicated for acetylacetone.[219] Such approaches also have the potential to more tightly integrate computation with experiment and to develop computational models that learn from experimental data.

Besides the actual number of points it is also relevant to consider the question what configurations of a system to use for the reference calculations. The points should be pace in the most informative regions, i.e. the regions the observables of interest are actually sensitive to. This question as already been discussed in another contribution to this special issue.[8]

For highly accurate, small molecule reaction dynamics based on represented *ab initio* calculated PESs one remaining challenge is the absence of a uniformly accurate and valid method to solve the electronic Schrödinger equation. While for single-reference problems coupled cluster (CC) techniques, such as CCSD(T), provide a valid "gold standard" such a generally applicable and robust technique is missing in regions of the PES for which a single-reference electronic wavefunction is not a good approximation. Multi-reference configuration interaction (MRCI) methods are a viable alternative but they are not yet of the same overall quality as CC-based techniques and they can be challenging to apply. Also, computing entire PESs with these methods can be non-trivial. It may be possible to apply mapping, scaling and compound techniques to blend different methods across a precomputed grid of interaction energies as has been done for example for N_3^-.[220] One possibility are multi reference coupled cluster (MRCC) methods although they remain computationally challenging,[221] in particular when global, full-dimensional PESs are required. On the other hand, full configuration interaction PESs have been computed for small, few-electron systems[222] and with increasing computer speed such calculations and systems become tractable.

Another area of future development concerns reactivity in electronically excited states. For small systems, *ab initio* calculations, ML-based representations of the PES and QCT dynamics simulations similar to ground state problems have been used for rate calculations for quite some time.[63,101,197,223,224] However, for larger systems, the dynamics in the excited state is a challenging problem in itself and ML-based techniques applied to this (nonreactive) problem only start to appear.[225] One particular point of concern is the non-adiabatic dynamics and the coupling matrix elements involved in the transition between neighbouring electronic states.[226,227]

It is expected that combining currently available ML techniques for fragmentation using mass spectrometry with advanced *ab initio* calculations and data from existing data bases (see Ref.[166]) will further boost the quantitative side of chemical structure determination from MS experiments. It is now possible to determine optimized structures for entire chemical libraries containing millions of compounds[165,228] at the density functional theory level of theory. Such information is potentially useful for better describing the reaction energetics of such decomposition and fragmentation processes and the relative importance of each of the channels.

Visualization and virtual reality techniques for exploration of chemical reactivity[229–232] are other areas in which ML-based techniques may become relevant.[233] Such approaches are likely to also become relevant in classroom chemistry,[233–236] A personal note is related to first viewing an MD simulation of myoglobin (using VMD) on a desktop screen as a postdoc working with Prof. M. Karplus, It was fascinating to follow the dance of atoms when nitric oxide was binding to and unbinding from the heme-iron.[237] Watching this reminded me immediately of the notion "..that everything that living things do can be understood in terms of the jigglings and wigglings of atoms."[238] The impression of this shaped my personal view of chemical and biological systems as inherently dynamical. Without capturing the dynamics

it was evident that a comprehensive understanding of chemical and biological function,[239] including enzymatic activity,[142] would not be possible. The combination of electronic structure theory, molecular dynamics, machine learning and virtual reality brings this one step closer and will also have potentially far reaching, transformative effects on the way how we will teach chemistry in the future.[240]

Machine learning techniques also have the potential to transform the way in which the community regards the relationship between experiment, simulation and theory. Together with automatization (robotics), the combination of ML, experiment and simulation bears the potential to develop integrated systems which optimize chemical reaction systems with respect to a particular task ("loss function"), such as maximizing yield, turnover, rate, or minimizing use of problematic solvent. One of the fields which has seen many advances is reaction planning for organic synthesis[145] although examples for such system optimization have been presented more than 20 years ago for gas-phase reaction dynamics.[241–243] in the context of "controlled chemistry".

In summary, ML-based approaches applied to chemical reactivity is a rapidly expanding field. The challenges ahead concern the accurate, quantitative and exhaustive determination of reaction outcomes, rates, and (internal) state distributions. Coupled with robotic platforms, reaction yields and reaction conditions can be optimized using ML and Bayesian techniques. In the field of enzyme design, appreciable improvements of turnover rates can be expected from coupling experiments with ML-based approaches and for protein-ligand interaction and recognition the recent advances made for protein structure prediction will provide important insights. Finally, exploring entire reaction networks has been possible very recently for specific processes (e.g. methane oxidation). Together with improved, high-quality reference data, exploration of chemical space for reactions relevant to combustion, atmospheric sciences and astrophysical chemistry will become viable.

Acknowledgment

I am pleased to acknowledge the contribution from many of my students and co- workers over the past decade to this research effort, in particular Ms. Upadhyay for assistance with Figure 5. I also thank Profs. J. M. Bowman, H. Guo, R. Krems, D. Wishart, N. Sahinidis, A. Aspuru-Guzik, and A. von Lilienfeld, and Dr. M. Aldeghi for correspondence. This work has been financially supported by the Swiss National Science Foundation (NCCR-MUST and Grant No. 200021-7117810), the AFOSR, and the University of Basel.

Author Biography

Markus Meuwly studied Physics at the University of Basel and completed his PhD in Physical Chemistry working with Prof. J. P. Maier. After postdocs with Prof. J. Hutson (Durham) and Prof. M. Karplus (Strasbourg and Harvard) as a Swiss National Science Foundation Postdoctoral Scholar he started as a Förderprofessor at the University of Basel in 2002 where he is Full Professor of Physical and Computational Chemistry. He also holds a visiting professorship at Brown University, Providence, RI. His scientific interests range from accurate intermolecular interactions based on multipolar, kernel- and neural network-based representations to applications of quantitative molecular simulations for cold (interstellar) and hot (hypersonics) environments and the investigation of the reactive dynamics and spectroscopy in proteins and in the condensed phase. Several of the tools are available in the CHARMM molecular simulation program.

References

(1) Vereecken, L.; Aumont, B.; Barnes, I.; Bozzelli, J.; Goldman, M.; Green, W.; Madronich, S.; McGillen, M.; Mellouki, A.; Orlando, J. et al. Perspective on mechanism development and structure-activity relationships for gas-phase atmospheric chemistry. *Int. J. Chem. Kinet.* **2018**, *50*, 435–469.

(2) Klippenstein, S. J. From theoretical reaction dynamics to chemical modeling of combustion. *Proceedings of the Combustion Institute* **2017**, *36*, 77–111.

(3) Wakelam, V.; Herbst, E.; Loison, J. C.; Smith, I. W. M.; Chandrasekaran, V.; Pavone, B.; Adams, N. G.; Bacchus-Montabonel, M. C.; Bergeat, A.; Beroff, K. et al. A kinetic database for astrochemistry (KIDA). *The Astrophysical Journal Supplement Series* **2012**, *199*, 21.

(4) van der Kamp, M. W.; Mulholland, A. J. Combined quantum mechanics/molecular mechanics (QM/MM) methods in computational enzymology. *Biophys. Chem.* **2013**, *52*, 2708–2728.

(5) Cheong, P. H.-Y.; Legault, C. Y.; Um, J. M.; Celebi-Ölcüm, N.; Houk, K. Quantum mechanical investigations of organocatalysis: mechanisms, reactivities, and selectivities. *Chem. Rev.* **2011**, *111*, 5042–5137.

(6) Koner, D.; Salehi, S. M.; Mondal, P.; Meuwly, M. Non-conventional force fields for applications in spectroscopy and chemical reaction dynamics. *J. Chem. Phys.* **2020**, *153*.

(7) Unke, O. T.; Chmiela, S.; Sauceda, H. E.; Gastegger, M.; Poltavsky, I.; Schütt, K. T.; Tkatchenko, A.; Müller, K.-R. Machine learning force fields. *arXiv preprint arXiv:2010.07067* **2020**,

(8) Manzhos, S.; Carrington Jr, T. Neural network potential energy surfaces for small molecules and reactions. *Chem. Rev.* **2020**, in print.

(9) Jiang, B.; Li, J.; Guo, H. High-Fidelity Potential Energy Surfaces for Gas-Phase and Gas- Surface Scattering Processes from Machine Learning. *J. Phys. Chem. Lett.* **2020**, *11*, 5120–5131.

(10) Cui, Q. Perspective: Quantum mechanical methods in biochemistry and biophysics. *J. Chem. Phys.* **2016**, *145*, 140901.

(11) Senn, H. M.; Thiel, W. QM/MM Methods for Biomolecular Systems. *Angew. Chem. Int. Ed.* **2009**, *48*, 1198–1229.

(12) Roston, D.; Demapan, D.; Cui, Q. Leaving Group Ability Observably Affects Transition State Structure in a Single Enzyme Active Site. *J. Am. Chem. Soc.* **2016**, *138*, 7386–7394.

(13) Kulik, H. J.; Zhang, J.; Klinman, J. P.; Martinez, T. J. How Large Should the QM Region Be in QM/MM Calculations? The Case of Catechol O-Methyltransferase. *J. Phys. Chem. B* **2016**, *120*, 11381–11394.

(14) Ellison, F. O. A method of diatomics in molecules. I. General theory and application to H2O. *J. Am. Chem. Soc.* **1963**, *85*, 3540–3544.

(15) Ellison, F. O.; Huff, N. T.; Patel, J. C. A Method of Diatomics in Molecules. II. H and H3+ 1. *J. Am. Chem. Soc.* **1963**, *85*, 3544–3547.

(16) Karplus, M.; Porter, R. N.; Sharma, R. D. Exchange Reactions with Activation Energy. I. Simple Barrier Potential for (H, H_2). *J. Chem. Phys.* **1965**, *43*, 3259–3287.

(17) Warshel, A.; Weiss, R. An Empirical Valence Bond Approach for Comparing Reactions in Solutions and in Enzymes. *J. Am. Chem. Soc.* **1980**, *102*, 6218–6226.

(18) Schmitt, U.; Voth, G. Multistate empirical valence bond model for proton transport in water. *J. Phys. Chem. B* **1998**, *102*, 5547–5551.

(19) van Duin, A.; Dasgupta, S.; Lorant, F.; Goddard, W. ReaxFF: A reactive force field for hydrocarbons. *J. Phys. Chem. A* **2001**, *105*, 9396–9409.

(20) Stoliarov, S. I.; Westmoreland, P. R.; Nyden, M. R.; Forney, G. P. A reactive molecular dynamics model of thermal decomposition in polymers: I. Poly (methyl methacrylate). *Polymer* **2003**, *44*, 883–894.

(21) Smith, K.; Stoliarov, S.; Nyden, M.; Westmoreland, P. RMDff: A smoothly transitioning, forcefield-based representation of kinetics for reactive molecular dynamics simulations. *Molecular Simulation* **2007**, *33*, 361–368.

(22) Nutt, D. R.; Meuwly, M. Studying reactive processes with classical dynamics: Rebinding dynamics in MbNO. *Biophys. J.* **2006**, *90*, 1191–1201.

(23) Danielsson, J.; Meuwly, M. Atomistic simulation of adiabatic reactive processes based on multi-state potential energy surfaces. *J. Chem. Theor. Comput.* **2008**, *4*, 1083–1093.

(24) Nagy, T.; Yosa Reyes, J.; Meuwly, M. Multisurface adiabatic reactive molecular dynamics. *J. Chem. Theor. Comput.* **2014**, *10*, 1366–1375.

(25) Schmid, M. H.; Das, A. K.; Landis, C. R.; Meuwly, M. Multi-State VALBOND for Atomistic Simulations of H ypervalent Molecules, Metal Complexes, and Reactions. *J. Chem. Theor. Comput.* **2018**, *14*, 3565–3578.

(26) Xu, Z.-H.; Meuwly, M. Multistate Reactive Molecular Dynamics Simulations of Proton Diffusion in Water Clusters and in the Bulk. *J. Phys. Chem. B* **2019**, *123*, 9846–9861.

(27) Farah, K.; Müller-Plathe, F.; Böhm, M. C. Classical reactive molecular dynamics implementations: State of the art. *Chem. Phys. Chem.* **2012**, *13*, 1127–1151.

(28) Collins, M. A. Molecular potential-energy surfaces for chemical reaction dynamics. *Theor. Chem. Acc.* **2002**, *108*, 313–324.

(29) Bowman, J. M.; Czako, G.; Fu, B. High-dimensional ab initio potential energy surfaces for reaction dynamics calculations. *Phys. Chem. Chem. Phys.* **2011**, *13*, 8094–8111.

(30) Hynes, J. T. Chemical reaction dynamics in solution. *Annu. Rev. Phys. Chem.* **1985**, *36*, 573–597.

(31) Hynes, J. T. Molecules in motion: chemical reaction and allied dynamics in solution and elsewhere. *Annual Review of Physical Chemistry* **2015**, *66*, 1–20.

(32) Warshel, A. Computer simulations of enzyme catalysis: methods, progress, and insights. *Annual review of biophysics and biomolecular structure* **2003**, *32*, 425–443.

(33) Gao, J.; Ma, S.; Major, D. T.; Nam, K.; Pu, J.; Truhlar, D. G. Mechanisms and free energies of enzymatic reactions. *Chem. Rev.* **2006**, *106*, 3188–3209.

(34) Himo, F. Recent trends in quantum chemical modeling of enzymatic reactions. *J. Am. Chem. Soc.* **2017**, *139*, 6780–6786.

(35) Amaro, R. E.; Mulholland, A. J. Multiscale methods in drug design bridge chemical and biological complexity in the search for cures. *Nature Reviews Chemistry* **2018**, *2*, 1–12.

(36) Arcus, V. L.; Mulholland, A. J. Temperature, Dynamics, and Enzyme-Catalyzed Reaction Rates. *Annual Review of Biophysics* **2020**, *49*, 163–180.

(37) Farah, K.; Leroy, F.; Müller-Plathe, F.; Böhm, M. C. Interphase formation during curing: reactive coarse grained molecular dynamics simulations. *J. Phys. Chem. C* **2011**, *115*, 16451–16460.

(38) Vapnik, V. N. *Statistical Learning Theory*; Wiley-Interscience, 1998.

(39) Minsky, M.; Papert, S. *Perceptrons; an Introduction to Computational Geometry*; MIT Press, 1969.

(40) Fukushima, K. Neocognitron - A Self-organizing Neural Network Model For A Mechanism Of Pattern-recognition Unaffected By Shift In Position. *Biological Cybernetics* **1980**, *36*, 193–202.

(41) Hopfield, J. Neural Networks And Physical Systems With Emergent Collective Computational Abilities. *Proc. Natl. Acad. Sci.* **1982**, *79*, 2554–2558.

(42) Linnainmaa, S. Taylor expansion of the accumulated rounding error. *BIT Numerical Mathematics* **1976**, *16*, 146–160.

(43) Rumelhart, D.; Hinton, G.; Williams, R. Learning Representations By Back-propagating Errors. *Nature* **1986**, *323*, 533–536.

(44) Werbos, P. Beyond regression:" new tools for prediction and analysis in the behavioral sciences. *Ph. D. dissertation, Harvard University* **1974**,

(45) Houston, P. L.; Nandi, A.; Bowman, J. M. A Machine Learning Approach for Prediction of Rate Constants. *J. Phys. Chem. Lett.* **2019**, *10*, 5250–5258.

(46) Nandi, A.; Bowman, J. M.; Houston, P. A Machine Learning Approach for Rate Constants. II. Clustering, Training, and Predictions for the $O(^3P)$+ HCl→OH+ Cl Reaction. *J. Phys. Chem. A* **2020**, *124*, 5746–5755.

(47) Komp, E.; Valleau, S. Machine Learning Quantum Reaction Rate Constants. *The Journal of Physical Chemistry A* **2020**, *124*, 8607–8613.

(48) Koner, D.; Unke, O. T.; Boe, K.; Bemish, R. J.; Meuwly, M. Exhaustive state-to-state cross sections for reactive molecular collisions from importance sampling simulation and a neural network representation. *J. Chem. Phys.* **2019**, *150*, 211101.

(49) Arnold, J.; Koner, D.; Kaeser, S.; Singh, N.; Bemish, R. J.; Meuwly, M. Machine Learning for Observables: Reactant to Product State Distributions for Atom-Diatom Collisions. *J. Phys. Chem. A* **2020**, *124*, 7177–7190.

(50) Schwaller, P.; Vaucher, A. C.; Laino, T.; Reymond, J.-L. Prediction of chemical reaction yields using deep learning. *ChemRxiv preprint doi* **2020**, *10*.

(51) Jorgensen, W. L.; Tirado-Rives, J. The OPLS potential functions for proteins - energy minimizations for crystals of cyclic-peptides and crambin. *J. Am. Chem. Soc.* **1988**, *110*, 1657–1666.

(52) MacKerell, A.; Bashford, D.; Bellott, M.; Dunbrack, R.; Evanseck, J.; Field, M.; Fischer, S.; Gao, J.; Guo, H.; Ha, S. et al. All-atom empirical potential for molecular modeling and dynamics studies of proteins. *J. Phys. Chem. B* **1998**, *102*, 3586–3616.

(53) Wang, J.; Wolf, R. M.; Caldwell, J. W.; Kollman, P. A.; Case, D. A. Development and testing of a general amber force field. *J. Comput. Chem.* **2004**, *25*, 1157–1174.

(54) Oostenbrink, C.; Villa, A.; Mark, A. E.; Van Gunsteren, W. F. A biomolecular force field based on the free enthalpy of hydration and solvation: the GROMOS force-field parameter sets 53A5 and 53A6. *J. Comp. Chem.* **2004**, *25*, 1656–1676.

(55) Ponder, J. W.; Wu, C.; Ren, P.; Pande, V. S.; Chodera, J. D.; Schnieders, M. J.; Haque, I.; Mobley, D. L.; Lambrecht, D. S.; DiStasio Jr, R. A. et al. Current status of the AMOEBA polarizable force field. *J. Phys. Chem. B* **2010**, *114*, 2549–2564.

(56) Kramer, C.; Gedeck, P.; Meuwly, M. Atomic Multipoles: Electrostatic Potential Fit, Local Reference Axis Systems and Conformational Dependence. *J. Comp. Chem.* **2012**, *33*, 1673–1688.

(57) Shi, Y.; Xia, Z.; Zhang, J.; Best, R.; Wu, C.; Ponder, J. W.; Ren, P. Polarizable atomic

multipole-based AMOEBA force field for proteins. *J. Chem. Theor. Comput.* **2013**, *9*, 4046–4063.

(58) Bereau, T.; Kramer, C.; Meuwly, M. Leveraging Symmetries of Static Atomic Multipole Electrostatics in Molecular Dynamics Simulations. *J. Chem. Theor. Comput.* **2013**, *9*, 5450–5459.

(59) Leven, I.; Hao, H.; Das, A. K.; Head-Gordon, T. A Reactive Force Field with Coarse-Grained Electrons for Liquid Water. *J. Phys. Chem. Lett.* **2020**, *11*, 9240–9247.

(60) McDaniel, J. G.; Schmidt, J. First-principles many-body force fields from the gas phase to liquid: A "universal" approach. *J. Phys. Chem. B* **2014**, *118*, 8042–8053.

(61) Kolb, B.; Marshall, P.; Zhao, B.; Jiang, B.; Guo, H. Representing Global Reactive Potential Energy Surfaces Using Gaussian Processes. *J. Phys. Chem. A* **2017**, *121*, 2552–2557.

(62) Koner, D.; Bemish, R. J.; Meuwly, M. Dynamics on Multiple Potential Energy Surfaces: Quantitative Studies of Elementary Processes Relevant to Hypersonics. *J. Phys. Chem. A* **2020**, *124*, 6255–6269.

(63) Koner, D.; Bemish, R. J.; Meuwly, M. The $C(^3P) + NO(X^2\Pi) \rightarrow O(^3P) + CN(X^2\Sigma^+)$, $N(^2D)/N(^4S) + CO(X^1\Sigma^+)$ reaction: Rates, branching ratios, and final states from 15 K to 20 000 K. *J. Chem. Phys.* **2018**, *149*, 094305.

(64) Hollebeek, T.; Ho, T.-S.; Rabitz, H. Constructing multidimensional molecular potential energy surfaces from ab initio data. *Annu. Rev. Phys. Chem.* **1999**, *50*, 537–570.

(65) Unke, O. T.; Meuwly, M. Toolkit for the Construction of Reproducing Kernel-Based Representations of Data: Application to Multidimensional Potential Energy Surfaces. *J. Chem. Inf. Model* **2017**, *57*, 1923–1931.

(66) Qu, C.; Yu, Q.; Bowman, J. M. Permutationally Invariant Potential Energy Surfaces. *Annu. Rev. Phys. Chem.* **2018**, *69*, 151–175.

(67) Behler, J.; Parrinello, M. Generalized Neural-Network Representation of High-Dimensional Potential-Energy Surfaces. *Phys. Rev. Lett.* **2007**, *98*, 146401.

(68) Schütt, K. T.; Sauceda, H. E.; Kindermans, P.-J.; Tkatchenko, A.; Müller, K.-R. SchNet–A deep learning architecture for molecules and materials. *J. Chem. Phys.* **2018**, *148*, 241722.

(69) Unke, O. T.; Meuwly, M. PhysNet: A Neural Network for Predicting Energies, Forces, Dipole Moments, and Partial Charges. *J. Chem. Theor. Comput.* **2019**, *15*, 3678–3693.

(70) Reactive dynamics and spectroscopy of hydrogen transfer from neural network-based reactive potential energy surfaces. *New J. Phys.* **2020**, *22*, 055002.

(71) Ho, T.-S.; Rabitz, H. A general method for constructing multidimensional molecular potential energy surfaces from ab initio calculations. *J. Chem. Phys.* **1996**, *104*, 2584–2597.

(72) Hollebeek, T.; Ho, T.-S.; Rabitz, H. A fast algorithm for evaluating multidimensional potential energy surfaces. *J. Chem. Phys.* **1997**, *106*, 7223–7227.

(73) Truhlar, D. G.; Muckerman, J. T. In *Atom - Molecule Collision Theory*; Bernstein, R. B., Ed.; Springer US, 1979; pp 505–566.

(74) Venturi, S.; Jaffe, R. L.; Panesi, M. Bayesian Machine Learning Approach to the Quantification of Uncertainties on Ab Initio Potential Energy Surfaces. *J. Phys. Chem. A* **2020**, *124*, 5129–5146.

(75) Boyd, I. D.; Schwartzentruber, T. E. *Nonequilibrium Gas Dynamics and Molecular Simulation*; Cambridge University Press, 2017; Vol. 42.

(76) Grover, M. S.; Torres, E.; Schwartzentruber, T. E. Direct molecular simulation of internal energy relaxation and dissociation in oxygen. *Phys. Fluid.* **2019**, *31*, 076107.

(77) He, K.; Zhang, X.; Ren, S.; Sun, J. *Deep Residual Learning for Image Recognition. Proceedings of the IEEE Conference on Computer Vision and Pattern Recognition.* **2016**, 770–778.

(78) Glorot, X.; Bengio, Y. Understanding the difficulty of training deep feedforward neural networks. Proceedings of the 13th International Conference on Artificial Intelligence and Statistics. 2010; pp 249–256.

(79) Nair, V.; Hinton, G. E. Rectified linear units improve restricted boltzmann machines. Proceedings of the 27th International Conference on Machine Learning. 2010; pp 807–814.

(80) Klambauer, G.; Unterthiner, T.; Mayr, A.; Hochreiter, S. Self-normalizing neural networks. *Advances in neural information processing systems* **2017**, *30*, 971–980.

(81) Unke, O. T.; Meuwly, M. A reactive, scalable, and transferable model for molecular energies from a neural network approach based on local information. *J. Chem. Phys.* **2018**, *148*, 241708.

(82) Kingma, D.; Ba, J. Adam: A method for stochastic optimization. *arXiv preprint arXiv:1412.6980* **2014**,

(83) Rasmussen, C. E.; Williams, C. K. I. *Gaussian Processes for Machine Learning,* `www.GaussianProcess.org`; MIT Press: Cambridge, 2006; Editor: T. Dietterich.

(84) Cui, J.; Krems, R. V. Efficient non-parametric fitting of potential energy surfaces for polyatomic molecules with Gaussian processes. *J. Phys. B: At. Mol. Opt. Phys.* **2016**, *49*, 224001.

(85) Krems, R. V. Bayesian machine learning for quantum molecular dynamics. *Phys. Chem. Chem. Phys.* **2019**, *21*, 13392–13410.

(86) Firsov, O. Determination Of Forces Acting Between Atoms With The Use Of The Differential Cross Section Of Elastic Scattering. *Zhur. Eksptl'. i Teoret Fiz.* **1953**, *24*.

(87) Buck, U.; Pauly, H. Determination Of Intermolecular Potentials By Inversion Of Molecular Beam Scattering Data. *J. Chem. Phys.* **1969**, *51*, 1662–1664.

(88) Buck, U. Inversion of molecular scattering data. *Rev. Mod. Phys.* **1974**, *46*, 369–389.

(89) Child, M.; Gerber, R. Inversion of inelastic atom-atom scattering data: recovery of the interaction function. *Mol. Phys.* **1979**, *38*, 421–432.

(90) Buck, U. Inversion Of Molecular-scattering Data. *Comp. Phys. Rep.* **1986**, *5*, 1–58.

(91) Boyd, R.; Ho, T.-S.; Rabitz, H. Determination of multiple diabatic potentials by the inversion of atom–atom scattering data. *J. Chem. Phys.* **1995**, *103*, 4052–4060.

(92) Vargas-Hernandez, R. A.; Guan, Y.; Zhang, D. H.; Krems, R., V Bayesian optimization for the inverse scattering problem in quantum reaction dynamics. *New J. Phys.* **2019**, *21*, 022001.

(93) Aronszajn, N. Theory of Reproducing Kernels. *Trans. Amer. Math. Soc.* **1950**, *68*, 337–404.

(94) Soldán, P.; Hutson, J. M. On the long-range and short-range behavior of potentials from reproducing kernel Hilbert space interpolation. *J. Chem. Phys.* **2000**, *112*, 4415–4416.

(95) Ho, T.; Rabitz, H.; Scoles, G. Reproducing kernel technique for extracting accurate potentials from spectral data: Potential curves of the two lowest states X $^1\Sigma_g^+$ and a $^3\Sigma_u^+$ of the sodium dimer. *J. Chem. Phys.* **2000**, *112*, 6218–6227.

(96) Hollebeek, T.; Ho, T.-S.; Rabitz, H. Efficient potential energy surfaces from partially filled ab initio data over arbitrarily shaped regions. *J. Chem. Phys.* **2001**, *114*, 3940–3944.

(97) Hollebeek, T.; Ho, T.-S.; Rabitz, H.; Harding, L. B. Construction of reproducing kernel Hilbert space potential energy surfaces for the $^1A''$ and $^1A'$ states of the reaction $N(^2D)+H_2$. *J. Chem. Phys.* **2001**, *114*, 3945–3948.

(98) Ho, T.-S.; Rabitz, H. Reproducing kernel Hilbert space interpolation methods as a paradigm of high dimensional model representations: Application to multidimensional potential energy surface construction. *J. Chem. Phys.* **2003**, *119*, 6433–6442.

(99) Luo, X.; Lu, Z.; Xu, X. Reproducing kernel technique for high dimensional model representations (HDMR). *Comput. Phys. Commun.* **2014**, *185*, 3099–3108.

(100) Soloviov, M.; Meuwly, M. Reproducing kernel potential energy surfaces in biomolecular simulations: Nitric oxide binding to myoglobin. *J. Chem. Phys.* **2015**, *143*, 105103.

(101) Koner, D.; Veliz, J. C. S. V.; Bemish, R. J.; Meuwly, M. Accurate Reproducing Kernel-Based Potential Energy Surfaces for the Triplet Ground States of N_2 O and Dynamics for the N+ NO $\leftrightarrow$ O+ N_2 and N_2+ O$\rightarrow$2N+O Reactions. *Phys. Chem. Chem. Phys.* **2020**, *22*, 18488–18498.

(102) Käser, S.; Koner, D.; Christensen, A. S.; von Lilienfeld, O. A.; Meuwly, M. ML Models of Vibrating H_2CO: Comparing Reproducing Kernels, FCHL and PhysNet. *arXiv preprint arXiv:2006.16752* **2020**,

(103) Koner, D.; Meuwly, M. Permutationally Invariant, Machine-Learned and Kernel-Based Potential Energy Surfaces for Polyatomic Molecules: From Formaldehyde to Acetone. *J. Chem. Theor. Comput.* **2020**, *16*, 5474–5484.

(104) Vargas-Hernandez, R. A.; Sous, J.; Berciu, M.; Krems, R. V. Extrapolating Quantum Observables with Machine Learning: Inferring Multiple Phase Transitions from Properties of a Single Phase. *Phys. Rev. Lett.* **2018**, *121*, 255702.

(105) Deng, Z.; Tutunnikov, I.; Averbukh, I. S.; Thachuk, M.; Krems, R. Bayesian optimization for inverse problems in time-dependent quantum dynamics. *arXiv preprint arXiv:2006.06212* **2020**,

(106) Dai, J.; Krems, R. V. Interpolation and extrapolation of global potential energy surfaces for polyatomic systems by Gaussian processes with composite kernels. *J. Chem. Theor. Comput.* **2020**, *16*, 1386–1395.

(107) Sugisawa, H.; Ida, T.; Krems, R. Gaussian process model of 51-dimensional potential energy surface for protonated imidazole dimer. *J. Chem. Phys.* **2020**, *153*, 114101.

(108) Li, J.; Zhao, B.; Xie, D.; Guo, H. Advances and New Challenges to Bimolecular Reaction Dynamics Theory. *J. Phys. Chem. Lett.* **2020**, *11*, 8844–8860.

(109) Olejnicak, J.; Candler, G. Vibrational-energy conservation with vibration-dissociation coupling - gneral theory and numberical studies. *Phys. Fluid.* **1995**, *7*, 1764–1774.

(110) Sarma, G. Physico-chemical modelling in hypersonic flow simulation. *Progr. Aerospace Sci.* **2000**, *36*, 281–349.

(111) Bertin, J.; Cummings, R. Fifty years of hypersonics: where we've been, where we're going. *Prog. Aerospace Sci.* **2003**, *39*, 511–536.

(112) Knight, D.; Longo, J.; Drikakis, D.; Gaitonde, D.; Lani, A.; Nompelis, I.; Reimann, B.; Walpot, L. Assessment of CFD capability for prediction of hypersonic shock interactions. *Progr. Aerospace Sci.* **2012**, *48-49*, 8–26.

(113) Leyva, I. The relentless pursuit of hypersonic flight. *Phys. Tod.* **2017**, *70*, 30–36.

(114) Wakelam, V.; Smith, I.; Herbst, E.; Troe, J.; Geppert, W.; Linnartz, H.; Öberg, K.; Roueff, E.; Agúndez, M.; Pernot, P. et al. Reaction networks for interstellar chemical modelling: improvements and challenges. *Space science reviews* **2010**, *156*, 13–72.

(115) Balucani, N. Elementary reactions and their role in gas-phase prebiotic chemistry. *International Journal of Molecular Sciences* **2009**, *10*, 2304–2335.

(116) Shaw, M. F.; Sztáray, B.; Whalley, L. K.; Heard, D. E.; Millet, D. B.; Jordan, M. J.; Osborn, D. L.; Kable, S. H. Photo-tautomerization of acetaldehyde as a photochemical source of formic acid in the troposphere. *Nat. Comm.* **2018**, *9*, 1–7.

(117) So, S.; Wille, U.; da Silva, G. Atmospheric Chemistry of Enols: A Theoretical Study of the Vinyl Alcohol + OH + O_2 Reaction Mechanism. *Environ. Sci. Technol* **2014**, *48*, 6694–6701.

(118) Archibald, A. T.; McGillen, M. R.; Taatjes, C. A.; Percival, C. J.; Shallcross, D. E. Atmospheric transformation of enols: A potential secondary source of carboxylic acids in the urban troposphere. *Geophys. Res. Lett.* **2007**, *34*, L21801.

(119) Andrews, D. U.; Heazlewood, B. R.; Maccarone, A. T.; Conroy, T.; Payne, R. J.; Jordan, M. J. T.; Kable, S. H. Photo-Tautomerization of Acetaldehyde to Vinyl Alcohol: A Potential Route to Tropospheric Acids. *Science* **2012**, *337*, 1203–1206.

(120) Clubb, A. E.; Jordan, M. J. T.; Kable, S. H.; Osborn, D. L. Phototautomerization of Acetaldehyde to Vinyl Alcohol: A Primary Process in UV-Irradiated Acetaldehyde from 295 to 335 nm. *J. Phys. Chem. Lett.* **2012**, *3*, 3522–3526.

(121) Millet, D. B.; Baasandorj, M.; Farmer, D. K.; Thornton, J. A.; Baumann, K.; Brophy, P.; Chaliyakunnel, S.; de Gouw, J. A.; Graus, M.; Hu, L. et al. A large and ubiquitous source of atmospheric formic acid. *Atmos. Chem. Phys* **2015**, *15*, 6283–6304.

(122) Käser, S.; Unke, O. T.; Meuwly, M. Isomerization and decomposition reactions of acetaldehyde relevant to atmospheric processes from dynamics simulations on neural network-based potential energy surfaces. *J. Chem. Phys.* **2020**, *152*, 214304.

(123) Reyes, J. Y.; Nagy, T.; Meuwly, M. Competitive reaction pathways in vibrationally induced photodissociation of H_2SO_4. *Phys. Chem. Chem. Phys.* **2014**, *16*, 18533–18544.

(124) Braams, B. J.; Bowman, J. M. Permutationally invariant potential energy surfaces in high dimensionality. *Int. Rev. Phys. Chem.* **2009**, *28*, 577–606.

(125) Jiang, B.; Li, J.; Guo, H. Potential energy surfaces from high fidelity fitting of ab initio points: the permutation invariant polynomial-neural network approach. *Int. Rev. Phys. Chem.* **2016**, *35*, 479–506.

(126) Li, J.; Chen, J.; Zhang, D. H.; Guo, H. Quantum and quasi-classical dynamics of the OH+ CO→H+ CO_2 reaction on a new permutationally invariant neural network potential energy surface. *J. Chem. Phys.* **2014**, *140*, 044327.

(127) Francisco, J. S.; Muckerman, J. T.; Yu, H.-G. HOCO radical chemistry. *Acc. Chem. Res.* **2010**, *43*, 1519–1526.

(128) Wagner, A. F.; Dawes, R.; Continetti, R. E.; Guo, H. Theoretical/experimental comparison of deep tunneling decay of quasi-bound H (D) OCO to H (D)+ CO2. *J. Chem. Phys.* **2014**, *141*, 054304.

(129) Jiang, B.; Guo, H. Six-dimensional quantum dynamics for dissociative chemisorption of H_2 and D_2 on Ag (111) on a permutation invariant potential energy surface. *Phys. Chem. Chem. Phys.* **2014**, *16*, 24704–24715.

(130) Jiang, B.; Hu, X.; Lin, S.; Xie, D.; Guo, H. Six-dimensional quantum dynamics of

dissociative chemisorption of H_2 on Co (0001) on an accurate global potential energy surface. *Phys. Chem. Chem. Phys.* **2015**, *17*, 23346–23355.

(131) Jiang, B.; Guo, H. Dynamics of water dissociative chemisorption on Ni (111): effects of impact sites and incident angles. *Phys. Rev. Lett.* **2015**, *114*, 166101.

(132) Jiang, B.; Guo, H. Communication: Enhanced dissociative chemisorption of CO2 via vibrational excitation. 2016.

(133) Weichman, M. L.; DeVine, J. A.; Babin, M. C.; Li, J.; Guo, L.; Ma, J.; Guo, H.; Neumark, D. M. Feshbach resonances in the exit channel of the F+ $CH_3OH \rightarrow$ HF+CH_3O reaction observed using transition-state spectroscopy. *Nat. Comm.* **2017**, *9*, 950.

(134) Lu, D.; Li, J.; Guo, H. Comprehensive investigations of the Cl+$CH_3OH \rightarrow$HCl+ CH_3O/CH_2OH reaction: validation of experiment and dynamic insights. *CCS Chemistry* **2020**, *2*, 882–894.

(135) Sweeny, B. C.; Pan, H.; Kassem, A.; Sawyer, J. C.; Ard, S. G.; Shuman, N. S.; Viggiano, A. A.; Brickel, S.; Unke, O. T.; Upadhyay, M. et al. Thermal activation of methane by MgO+: temperature dependent kinetics, reactive molecular dynamics simulations and statistical modeling. *Phys. Chem. Chem. Phys.* **2020**, *22*, 8913–8923.

(136) Kidwell, N. M.; Li, H.; Wang, X.; Bowman, J. M.; Lester, M. I. Unimolecular dissociation dynamics of vibrationally activated CH_3CHOO Criegee intermediates to OH radical products. *Nat. Comm.* **2016**, *8*, 509–514.

(137) Fang, Y.; Liu, F.; Barber, V. P.; Klippenstein, S. J.; McCoy, A. B.; Lester, M. I. Communication: Real time observation of unimolecular decay of Criegee intermediates to OH radical products. 2016.

(138) Soloviov, M.; Das, A. K.; Meuwly, M. Structural Interpretation of Metastable States in Myoglobin-NO. *Angew. Chem. Int. Ed.* **2016**, *55*, 10126–10130.

(139) Kiss, G.; Çelebi-Ölçüm, N.; Moretti, R.; Baker, D.; Houk, K. Computational enzyme design. *Angew. Chem. Int. Ed.* **2013**, *52*, 5700–5725.

(140) Senior, A. W.; Evans, R.; Jumper, J.; Kirkpatrick, J.; Sifre, L.; Green, T.; Qin, C.; Zidek, A.; Nelson, A. W. R.; Bridgland, A. et al. Improved protein structure prediction using potentials from deep learning. *Nature* **2020**, *577*, 706–710.

(141) AlphaFold: a solution to a 50-year-old grand challenge in biology. `https://deepmind.com/blog/article/alphafold-a-solution-to-a-50-year-old-grand-challenge-in-biology/`, Accessed: 2020-12-29.

(142) Otten, R.; Pádua, R. A.; Bunzel, H. A.; Nguyen, V.; Pitsawong, W.; Patterson, M.; Sui, S.; Perry, S. L.; Cohen, A. E.; Hilvert, D. et al. How directed evolution reshapes the energy landscape in an enzyme to boost catalysis. *Science* **2020**, *370*, 1442–1446.

(143) Privett, H. K.; Kiss, G.; Lee, T. M.; Blomberg, R.; Chica, R. A.; Thomas, L. M.; Hilvert, D.; Houk, K. N.; Mayo, S. L. Iterative approach to computational enzyme design. *Proc. Natl. Acad. Sci.* **2012**, *109*, 3790–3795.

(144) Wei, J. N.; Duvenaud, D.; Aspuru-Guzik, A. Neural Networks for the Prediction of Organic Chemistry Reactions. *Acs Central Science* **2016**, *2*, 725–732.

(145) Filipa de Almeida, A.; Moreira, R.; Rodrigues, T. Synthetic organic chemistry driven by artificial intelligence. *Nat. Rev. Chem.* **2019**, *3*, 589–604.

(146) Zhou, Z.; Li, X.; Zare, R. N. Optimizing chemical reactions with deep reinforcement learning. *ACS central science* **2017**, *3*, 1337–1344.

(147) Gao, H.; Struble, T. J.; Coley, C. W.; Wang, Y.; Green, W. H.; Jensen, K. F. Using Machine Learning To Predict Suitable Conditions for Organic Reactions. *ACS Central Science* **2018**, *4*, 1465–1476.

(148) Allen, F.; Pon, A.; Greiner, R.; Wishart, D. Computational prediction of electron ionization mass spectra to assist in GC/MS compound identification. *Anal. Chem.* **2016**, *88*, 7689–7697.

(149) Dührkop, K.; Nothias, L.-F.; Fleischauer, M.; Reher, R.; Ludwig, M.; Hoffmann, M. A.; Petras, D.; Gerwick, W. H.; Rousu, J.; Dorrestein, P. C. et al. Systematic classification of unknown metabolites using high-resolution fragmentation mass spectra. *Nature Biotechnology* **2020**, 1–10.

(150) Vléduts, G.; Finn, V. Creating a machine language for organic chemistry. *Information Storage and Retrieval* **1963**, *1*, 101–116.

(151) Corey, E. J. General methods for the construction of complex molecules. *Pure Appl. Chem* **1967**, *14*, 19–38.

(152) Corey, E.; Wipke, W. Computer-assisted Design Of Complex Organic Syntheses. *Science* **1969**, *166*, 178–192.

(153) Hendrickson, J. B. Systematic characterization of structures and reactions for use in organic synthesis. *J. Am. Chem. Soc.* **1971**, *93*, 6847–6854.

(154) Gelernter, H.; Sridharan, N. S.; Hart, A. J.; Yen, S.-C.; Fowler, F. W.; Shue, H.-J. *New Concepts I*; Springer, 1973; pp 113–150.

(155) Gelernter, H.; Sanders, A.; Larsen, D.; Agarwal, K.; Boivie, R.; Spritzer, G.; Searleman, J. Empirical explorations of SYNCHEM. *Science* **1977**, *197*, 1041–1049.

(156) Salatin, T. D.; Jorgensen, W. L. Computer-assisted mechanistic evaluation of organic reactions. 1. Overview. *J. Org. Chem.* **1980**, *45*, 2043–2051.

(157) Lederberg, J. Topological mapping of organic molecules. *Proc. Natl. Acad. Sci.* **1965**, *53*, 134–139.

(158) Lindsay, R. K.; Buchanan, B. G.; Feigenbaum, E. A.; Lederberg, J. DENDRAL: a case study of the first expert system for scientific hypothesis formation. *Artificial intelligence* **1993**, *61*, 209–261.

(159) Lederberg, J.; Sutherland, G. L.; Buchanan, B. G.; Feigenbaum, E. A.; Robertson, A. V.; Duffield, A. M.; Djerassi, C. Applications of artificial intelligence for chemical inference. I. Number of possible organic compounds. Acyclic structures containing carbon, hydrogen, oxygen, and nitrogen. *J. Am. Chem. Soc.* **1969**, *91*, 2973–2976.

(160) Jorgensen, W. L.; Laird, E. R.; Gushurst, A. J.; Fleischer, J. M.; Gothe, S. A.; Helson, H. E.; Paderes, G. D.; Sinclair, S. CAMEO: a program for the logical prediction of the products of organic reactions. *Pure and Applied Chemistry* **1990**, *62*, 1921–1932.

(161) Gasteiger, J.; Hutchings, M. G.; Christoph, B.; Gann, L.; Hiller, C.; Löw, P.; Marsili, M.; Saller, H.; Yuki, K. *Organic Synthesis, Reactions and Mechanisms*; Springer, 1987; pp 19–73.

(162) Kayala, M. A.; Baldi, P. ReactionPredictor: prediction of complex chemical reactions at the mechanistic level using machine learning. *J. Chem. Inf. Model.* **2012**, *52*, 2526–2540.

(163) Skoraczyński, G.; Dittwald, P.; Miasojedow, B.; Szymkuć, S.; Gajewska, E.; Grzybowski, B. A.; Gambin, A. Predicting the outcomes of organic reactions via machine learning: are current descriptors sufficient? *Sci. Rep.* **2017**, *7*, 1–9.

(164) Szymkuć, S.; Gajewska, E. P.; Klucznik, T.; Molga, K.; Dittwald, P.; Startek, M.; Bajczyk, M.; Grzybowski, B. A. Computer-Assisted Synthetic Planning: The End of the Beginning. *Angew. Chem. Int. Ed.* **2016**, *55*, 5904–5937.

(165) Smith, J. S.; Isayev, O.; Roitberg, A. E. ANI-1: an extensible neural network potential with DFT accuracy at force field computational cost. *Chem. Sci.* **2017**, *8*, 3192–3203.

(166) Huang, B.; von Lilienfeld, O. A. Quantum machine learning in chemical compound space. *arXiv preprint arXiv:2012.07502* **2020**,

(167) Lim, H.; Jung, Y. Delfos: deep learning model for prediction of solvation free energies in generic organic solvents. *Chem. Sci.* **2019**, *10*, 8306–8315.

(168) Basdogan, Y.; Groenenboom, M. C.; Henderson, E.; De, S.; Rempe, S. B.; Keith, J. A. Machine learning-guided approach for studying solvation environments. *J. Chem. Theor. Comput.* **2019**, *16*, 633–642.

(169) Rauer, C.; Bereau, T. Hydration free energies from kernel-based machine learning: Compound-database bias. *J. Chem. Phys.* **2020**, *153*, 014101.

(170) Scheen, J.; Wu, W.; Mey, A. S.; Tosco, P.; Mackey, M.; Michel, J. Hybrid Alchemical Free Energy/Machine-Learning Methodology for the Computation of Hydration Free Energies. *J. Chem. Inf. Model.* **2020**, *60*, 5331–5339.

(171) Steiner, S.; Wolf, J.; Glatzel, S.; Andreou, A.; Granda, J. M.; Keenan, G.; Hinkley, T.; Aragon-Camarasa, G.; Kitson, P. J.; Angelone, D. et al. Organic synthesis in a modular robotic system driven by a chemical programming language. *Science* **2019**, *363*.

(172) Coley, C. W.; Thomas, D. A.; Lummiss, J. A.; Jaworski, J. N.; Breen, C. P.; Schultz, V.; Hart, T.; Fishman, J. S.; Rogers, L.; Gao, H. et al. A robotic platform for flow synthesis of organic compounds informed by AI planning. *Science* **2019**, *365*, eaax1566.

(173) Roch, L. M.; Häse, F.; Kreisbeck, C.; Tamayo-Mendoza, T.; Yunker, L. P.; Hein, J. E.; Aspuru-Guzik, A. ChemOS: Orchestrating autonomous experimentation. *Science Robotics* **2018**, *3*.

(174) Flores-Leonar, M. M.; Mejía-Mendoza, L. M.; Aguilar-Granda, A.; Sanchez-Lengeling, B.; Tribukait, H.; Amador-Bedolla, C.; Aspuru-Guzik, A. Materials Ac-

celeration Platforms: On the way to autonomous experimentation. *Current Opinion in Green and Sustainable Chemistry* **2020**, 100370.

(175) Hase, F.; Roch, L. M.; Kreisbeck, C.; Aspuru-Guzik, A. Phoenics: A Bayesian Optimizer for Chemistry. *Acs Central Science* **2018**, *4*, 1134–1145.

(176) Häse, F.; Roch, L. M.; Aspuru-Guzik, A. Gryffin: An algorithm for Bayesian optimization for categorical variables informed by physical intuition with applications to chemistry. *arXiv preprint arXiv:2003.12127* **2020**,

(177) Wilson, Z. T.; Sahinidis, N. V. Automated learning of chemical reaction networks. *Computers & Chemical Engineering* **2019**, *127*, 88–98.

(178) Maddison, C. J.; Mnih, A.; Teh, Y. W. The concrete distribution: A continuous relaxation of discrete random variables. *arXiv preprint arXiv:1611.00712* **2016**,

(179) Jang, E.; Gu, S.; Poole, B. Categorical reparameterization with gumbel-softmax. *arXiv preprint arXiv:1611.01144* **2016**,

(180) Christensen, M.; Yunker, L.; Adedeji, F.; Häse, F.; Roch, L.; Gensch, T.; dos Passos Gomes, G.; Zepel, T.; Sigman, M.; Aspuru-Guzik, A. et al. Data-science driven autonomous process optimization. **2020**,

(181) Gasteiger, J.; Hanebeck, W.; Schulz, K.-P. Prediction of mass spectra from structural information. *J. Chem. Inf. Com. Sci.* **1992**, *32*, 264–271.

(182) Allen, F.; Pon, A.; Wilson, M.; Greiner, R.; Wishart, D. CFM-ID: a web server for annotation, spectrum prediction and metabolite identification from tandem mass spectra. *Nucleic acids research* **2014**, *42*, W94–w99.

(183) Dührkop, K.; Shen, H.; Meusel, M.; Rousu, J.; Böcker, S. Searching molecular structure databases with tandem mass spectra using CSI: FingerID. *Proc. Natl. Acad. Sci.* **2015**, *112*, 12580–12585.

(184) Feunang, Y. D.; Eisner, R.; Knox, C.; Chepelev, L.; Hastings, J.; Owen, G.; Fahy, E.; Steinbeck, C.; Subramanian, S.; Bolton, E. et al. ClassyFire: automated chemical classification with a comprehensive, computable taxonomy. *J. Cheminf.* **2016**, *8*, 61.

(185) Heinonen, M.; Shen, H.; Zamboni, N.; Rousu, J. Metabolite identification and molecular fingerprint prediction through machine learning. *Bioinformatics* **2012**, *28*, 2333–2341.

(186) Shen, H.; Dührkop, K.; Böcker, S.; Rousu, J. Metabolite identification through multiple kernel learning on fragmentation trees. *Bioinformatics* **2014**, *30*, i157–i164.

(187) Böcker, S.; Dührkop, K. Fragmentation trees reloaded. *Journal of cheminformatics* **2016**, *8*, 5.

(188) Matthews, B. W. Comparison of the predicted and observed secondary structure of T4 phage lysozyme. *Biochimica et Biophysica Acta (BBA)-Protein Structure* **1975**, *405*, 442–451.

(189) Gillespie, D. T. Stochastic simulation of chemical kinetics. *Annu. Rev. Phys. Chem.* **2007**, *58*, 35–55.

(190) Wang, L.-P.; Titov, A.; McGibbon, R.; Liu, F.; Pande, V. S.; Martínez, T. J. Discovering chemistry with an ab initio nanoreactor. *Nat. Comm.* **2014**, *6*, 1044–1048.

(191) Zeng, J.; Cao, L.; Xu, M.; Zhu, T.; Zhang, J. Z. Complex reaction processes in combustion unraveled by neural network-based molecular dynamics simulation. *Nature communications* **2020**, *11*, 1–9.

(192) Zhang, L.; Han, J.; Wang, H.; Car, R.; Weinan, E. Deep potential molecular dynamics: a scalable model with the accuracy of quantum mechanics. *Phys. Rev. Lett.* **2018**, *120*, 143001.

(193) Stocker, S.; Csanyi, G.; Reuter, K.; Margraf, J. T. Machine learning in chemical reaction space. *Nat. Comm.* **2020**, *11*, 5505.

(194) Bartók, A. P.; Kondor, R.; Csányi, G. On representing chemical environments. *Physical Review B* **2013**, *87*, 184115.

(195) Cozad, A.; Sahinidis, N. V.; Miller, D. C. Learning surrogate models for simulation-based optimization. *AIChE Journal* **2014**, *60*, 2211–2227.

(196) Loeppky, J. L.; Sacks, J.; Welch, W. J. Choosing the sample size of a computer experiment: A practical guide. *Technometrics* **2009**, *51*, 366–376.

(197) San Vicente Veliz, J. C.; Koner, D.; Schwilk, M.; Bemish, R. J.; Meuwly, M. The $N(^4S) + O_2(X^3\Sigma_g^-) \leftrightarrow O(^3P) + NO(X^2\Pi)$ Reaction: Thermal and Vibrational Relaxation Rates for the $^2A'$, $^4A'$ and $^2A''$ States. *Phys. Chem. Chem. Phys.* **2020**, *22*, 3927–3939.

(198) Kennedy, M. C.; O'Hagan, A. Bayesian calibration of computer models. *Journal of the Royal Statistical Society: Series B (Statistical Methodology)* **2001**, *63*, 425–464.

(199) Heo, H.; Ho, T.-S.; Lehmann, K. K.; Rabitz, H. Regularized inversion of diatomic vibration–rotation spectral data: A functional sensitivity analysis approach. *J. Chem. Phys.* **1992**, *97*, 852–861.

(200) Meuwly, M.; Hutson, J. Morphing ab initio potentials: A systematic study of Ne-HF. *J. Chem. Phys.* **1999**, *110*, 8338–8347.

(201) Gazdy, B.; Bowman, J. An Adjusted Global Potential Surface For HCN Based On Rigorous Vibrational Calculations. *J. Chem. Phys.* **1991**, *95*, 6309–6316.

(202) McIntosh, A.; Wang, Z.; Castillo-Chara, J.; Lucchese, R.; Bevan, J.; Suenram, R.; Legon, A. The structure and ground state dynamics of Ar-IH. *J. Chem. Phys.* **1999**, *111*, 5764–5770.

(203) Lorenz, K.; Westley, M.; Chandler, D. Rotational state-to-state differential cross sections for the HCl-Ar collision system using velocity-mapped ion imaging. *Phys. Chem. Chem. Phys.* **2000**, *2*, 481–494.

(204) Xu, Y.; Jager, W. The dynamics of the CO-N_2 interaction: Strong Coriolis coupling in CO-paraN_2. *J. Chem. Phys.* **2000**, *113*, 514–524.

(205) Castillo-Chara, J.; Lucchese, R.; Bevan, J. Differentiation of the ground vibrational and global minimum structures in the Ar : HBr intermolecular complex. *J. Chem. Phys.* **2001**, *115*, 899–911.

(206) Kerenskaya, G.; Kaledin, A.; Heaven, M. Potential energy surfaces for CH(A $^2\Delta$)-Ar and analysis of the A $^2\Delta$ $X^2\Pi$ band system. *J. Chem. Phys.* **2001**, *115*, 2123–2133.

(207) van Mourik, T.; Harris, G.; Polyansky, O.; Tennyson, J.; Csaszar, A.; Knowles, P. Ab initio global potential, dipole, adiabatic, and relativistic correction surfaces for the HCN-HNC system. *J. Chem. Phys.* **2001**, *115*, 3706–3718.

(208) Shroll, R.; Lohr, L.; Barker, J. Empirical potentials for rovibrational energy transfer of hydrogen fluoride in collisions with argon. *J. Chem. Phys.* **2001**, *115*, 4573–4585.

(209) Howson, J.; Hutson, J. Morphing the He-OCS intermolecular potential. *J. Chem. Phys.* **2001**, *115*, 5059–5065.

(210) Shirin, S.; Polyansky, O.; Zobov, N.; Barletta, P.; Tennyson, J. Spectroscopically determined potential energy surface of (H_2O)-O^{16} up to 25 000 cm^{-1}. *J. Chem. Phys.* **2003**, *118*, 2124–2129.

(211) Xu, D.; Guo, H.; Zou, S.; Bowman, J. A scaled ab initio potential energy surface for acetylene and vinylidene. *Chem. Phys. Lett.* **2003**, *377*, 582–588.

(212) Bowman, J.; Xantheas, S. "Morphing" of ab initio-based interaction potentials to spectroscopic accuracy: Application to Cl-(H_2O). *Pure And Applied Chemistry* **2004**, *76*, 29–35.

(213) McElmurry, B.; Lucchese, R.; Bevan, J.; Belov, S. Analysis of the submillimetre Ar : HI Sigma bending transition as a test of a morphed potential. *Phys. Chem. Chem. Phys.* **2004**, *6*, 5318–5323.

(214) Wang, Z.; Lucchese, R.; Bevan, J. A Kr-BrH global minimum structure determined on the basis of potential morphing. *J. Phys. Chem. A* **2004**, *108*, 2884–2892.

(215) Rivera-Rivera, L. A.; Lucchese, R. R.; Bevan, J. W. A parameterized compound-model chemistry for morphing the intermolecular potential of OC-HCl. *Chem. Phys. Lett.* **2008**, *460*, 352–358.

(216) Spirko, V. Morphing ab initio potential energy curve of beryllium monohydride. *J. Mol. Struct.* **2016**, *330*, 89–95.

(217) Yurchenko, S. N.; Lodi, L.; Tennyson, J.; Stolyarov, A. V. Duo: a general program for calculating spectra of diatomic molecules. *Comput. Phys. Commun.* **2016**, *202*, 262–275.

(218) Augustovicova, L. D.; Spirko, V. Morphing radial molecular property functions of hydroxyl. *Journal Of Quantitative Spectroscopy & Radiative Transfer* **2020**, *254*, 107211.

(219) Qu, C.; Conte, R.; Houston, P. L.; Bowman, J. M. Full-dimensional potential energy surface for acetylacetone and tunneling splittings. *Phys. Chem. Chem. Phys.* **2020**,

(220) Sebald, P.; Stein, C.; Oswald, R.; Botschwina, P. Rovibrational States of N_3^--and CO_2 Up to High J: A Theoretical Study Beyond fc-CCSD(T). *J. Phys. Chem. A* **2013**, *117*, 13806–13814.

(221) Evangelista, F. A. Perspective: Multireference coupled cluster theories of dynamical electron correlation. *J. Chem. Phys.* **2018**, *149*, 030901.

(222) Koner, D.; San Vicente Veliz, J. C.; van der Avoird, A.; Meuwly, M. Near dissociation states for H_2^+–He on MRCI and FCI potential energy surfaces. *Phys. Chem. Chem. Phys.* **2019**, *21*, 24976–24983.

(223) Castro-Palacio, J. C.; Nagy, T.; Bemish, R. J.; Meuwly, M. Computational study of collisions between O(^3P) and NO($^2\Pi$) at temperatures relevant to the hypersonic flight regime. *J. Chem. Phys.* **2014**, *141*, 164319.

(224) Denis-Alpizar, O.; Bemish, R. J.; Meuwly, M. Reactive collisions for NO((II)-I-2) + N(S-4) at temperatures relevant to the hypersonic flight regime. *Phys. Chem. Chem. Phys.* **2017**, *19*, 2392–2401.

(225) Westermayr, J.; Gastegger, M.; Marquetand, P. Combining SchNet and SHARC: The SchNarc machine learning approach for excited-state dynamics. *J. Phys. Chem. Lett.* **2020**, *11*, 3828–3834.

(226) Tully, J. C. Perspective: Nonadiabatic dynamics theory. *J. Chem. Phys.* **2012**, *137*, 22A301.

(227) Guo, H.; Yarkony, D. R. Accurate nonadiabatic dynamics. *Phys. Chem. Chem. Phys.* **2016**, *18*, 26335–26352.

(228) Fink, T.; Reymond, J.-L. Virtual exploration of the chemical universe up to 11 atoms of C, N, O, F: assembly of 26.4 million structures (110.9 million stereoisomers) and analysis for new ring systems, stereochemistry, physicochemical properties, compound classes, and drug discovery. *J. Chem. Inf. Model.* **2007**, *47*, 342–353.

(229) Atkinson, W. D.; Bond, K. E.; Tribble III, G. L.; Wilson, K. R. Computing with feeling. *Computers & Graphics* **1977**, *2*, 97–103.

(230) Stone, J. E.; Gullingsrud, J.; Schulten, K. A system for interactive molecular dynamics simulation. Proceedings of the 2001 symposium on Interactive 3D graphics. 2001; pp 191–194.

(231) Martínez, T. J. Ab initio reactive computer aided molecular design. *Acc. Chem. Res.* **2017**, *50*, 652–656.

(232) Haag, M. P.; Vaucher, A. C.; Bosson, M.; Redon, S.; Reiher, M. Interactive chemical reactivity exploration. *Comput. Phys. Commun.* **2014**, *15*, 3301–3319.

(233) O'Connor, M. B.; Bennie, S. J.; Deeks, H. M.; Jamieson-Binnie, A.; Jones, A. J.; Shannon, R. J.; Walters, R.; Mitchell, T. J.; Mulholland, A. J.; Glowacki, D. R. Interactive molecular dynamics in virtual reality from quantum chemistry to drug binding: An open-source multi-person framework. *J. Chem. Phys.* **2019**, *150*, 220901.

(234) Aspuru-Guzik, A.; Lindh, R.; Reiher, M. The matter simulation (r) evolution. *ACS central science* **2018**, *4*, 144–152.

(235) Martino, M.; Salvadori, A.; Lazzari, F.; Paoloni, L.; Nandi, S.; Mancini, G.; Barone, V.; Rampino, S. Chemical promenades: Exploring potential-energy surfaces with immersive virtual reality. *J. Comp. Chem.* **2020**, *41*, 1310–1323.

(236) Juul, J. Virtual Reality: Fictional all the Way Down (and that's OK). *Disputatio-international Journal Of Philosophy* **2019**, *11*, 333–343.

(237) Meuwly, M.; Becker, O.; Stote, R.; Karplus, M. NO rebinding to myoglobin: a reactive molecular dynamics study. *Biophys. Chem.* **2002**, *98*, 183–207.

(238) Feynman, R. P.; Leighton, R. B.; Sands, M. The feynman lectures on physics; vol. i. *American Journal of Physics* **1965**, *33*, 750–752.

(239) van der Kamp, M. W.; Prentice, E. J.; Kraakman, K. L.; Connolly, M.; Mulholland, A. J.; Arcus, V. L. Dynamical origins of heat capacity changes in enzyme-catalysed reactions. *Nat. Comm.* **2018**, *9*, 1–7.

(240) Amabilino, S.; Bratholm, L. A.; Bennie, S. J.; VaucherM, A. C.; Reiher, M.; Glowacki, D. R. Training Neural Nets To Learn Reactive Potential Energy Surfaces Using Interactive Quantum Chemistry in Virtual Reality. *J. Phys. Chem. A* **2019**, *123*, 4486–4499.

(241) Judson, R.; Rabitz, H. Teaching Lasers to Control Molecules. *Phys. Rev. Lett.* **1992**, *68*, 1500–1503.

(242) Roslund, J.; Shir, O. M.; Dogariu, A.; Miles, R.; Rabitz, H. Control of nitromethane photoionization efficiency with shaped femtosecond pulses. *J. Chem. Phys.* **2011**, *134*, 154301.

(243) Dong, D.; Xing, X.; Ma, H.; Chen, C.; Liu, Z.; Rabitz, H. Learning-Based Quantum Robust Control: Algorithm, Applications, and Experiments. *IEEE Trans. Cybern.* **2020**, *50*, 3581–3593.